A multiplier peroxiporin signal transduction pathway powers piscine spermatozoa

François Chauvigné[a], Carla Ducat[a], Alba Ferré[a], Tom Hansen[b], Montserrat Carrascal[c], Joaquín Abián[c], Roderick Nigel Finn[a,d], and Joan Cerdà[a,1]

[a]Institute of Agrifood Research and Technology, Institute of Biotechnology and Biomedicine, Universitat Autònoma de Barcelona, 08193 Barcelona, Spain; [b]Institute of Marine Research, Matre Aquaculture Research Station, 5984 Matredal, Norway; [c]Consejo Superior de Investigaciones Cientificas/Universitat Autònoma de Barcelona Proteomics Laboratory, Instituto de Investigaciones Biomédicas de Barcelona-Consejo Superior de Investigaciones Cientificas-August Pi i Sunyer Biomedical Research Institute, 08193 Barcelona, Spain; and [d]Department of Biology, Bergen High Technology Centre, University of Bergen, 5020 Bergen, Norway

Edited by Mariana F. Wolfner, Cornell University, Ithaca, NY, and approved January 26, 2021 (received for review September 17, 2020)

The primary task of a spermatozoon is to deliver its nuclear payload to the egg to form the next-generation zygote. With polyandry repeatedly evolving in the animal kingdom, however, sperm competition has become widespread, with the highest known intensities occurring in fish. Yet, the molecular controls regulating spermatozoon swimming performance in these organisms are largely unknown. Here, we show that the kinematic properties of postactivated piscine spermatozoa are regulated through a conserved trafficking mechanism whereby a peroxiporin ortholog of mammalian aquaporin-8 (Aqp8bb) is inserted into the inner mitochondrial membrane to facilitate H_2O_2 efflux in order to maintain ATP production. In teleosts from more ancestral lineages, such as the zebrafish (*Danio rerio*) and the Atlantic salmon (*Salmo salar*), in which spermatozoa are activated in freshwater, an intracellular Ca^{2+}-signaling directly regulates this mechanism through monophosphorylation of the Aqp8bb N terminus. In contrast, in more recently evolved marine teleosts, such the gilthead seabream (*Sparus aurata*), in which spermatozoa activation occurs in seawater, a cross-talk between Ca^{2+}- and oxidative stress-activated pathways generate a multiplier regulation of channel trafficking via dual N-terminal phosphorylation. These findings reveal that teleost spermatozoa evolved increasingly sophisticated detoxification pathways to maintain swimming performance under a high osmotic stress, and provide insight into molecular traits that are advantageous for postcopulatory sexual selection.

aquaporin | mitochondria | sperm | oxidative stress | sexual selection

For many dioecious animals, spermatozoon velocity, progressivity, and duration of motility are vital determinants of reproductive success and are thus major selection criteria for sperm evolution (1–6). Maximizing such kinematic properties contributes to spermatozoon vigor (7); however, due to the limitations in sperm ATP stores, which provide the chemical energy for flagellar contractions, a trade-off between swimming fast and for extended periods typically exists (8). Optimal combinations of traits that improve spermatozoon vigor are nevertheless important in polyandrous vertebrates facing sperm competition, which represents a powerful form of postcopulatory sexual selection (9–15). Since the phenomenon of sperm competition was first recognized (16), investigators have sought to understand the underlying mechanisms that could explain advantageous trait selection (17). To date, however, most research has focused on the physical and morphological properties involved in sperm competition, and very little is known concerning the molecular and genetic mechanisms underpinning spermatozoon performance (15, 18, 19).

One positively selected morphological change in respect of spermatozoon velocity and longevity in vertebrates as diverse as fishes, birds, and mammals, has been the increase in the spermatozoon midpiece size and the number or scale of mitochondria therein (20–22). Such changes have logically been associated with increased mitochondrial production of ATP for improved flagellar motility. However, the biochemical reactions that lead to increased ATP synthesis also generate elevated levels of hydrogen peroxide (H_2O_2), a reactive oxygen species (ROS) that inhibits mitochondrial function and suppresses flagellar motility (23–27). With osmotic stress of the exposed ejaculate generating additional ROS (26, 28), it has been unclear how sperm evolved molecular mechanisms that surmount such signaling conflicts.

A solution to this apparent paradox was recently discovered in the spermatozoa of a marine teleost, in which a water channel protein, now termed Aqp8bb (a peroxiporin ortholog of mammalian aquaporin-8) (29), is rapidly (<1 s) trafficked to the inner mitochondrial membrane upon activation in seawater (SW) to facilitate H_2O_2 efflux and the maintenance of ATP production and flagellar motility (26). The importance of Aqp8bb, which mainly functions as a peroxiporin in these germ cells, was demonstrated through immunological inhibitory experiments, which highlighted the channel-trafficking mechanism as a critical regulator of the spermatozoon velocity and motility (26). To date, however, the signal transduction pathways that regulate peroxiporin trafficking in vertebrate spermatozoa remain completely unknown.

Among externally fertilizing vertebrates, the highest known intensity of sperm competition occurs in true bony fishes (teleosts) (6), and we therefore focused our investigations on these model organims. In contrast to amniotic vertebrates, in which ejaculates become gelatinous when emitted (30), the ejaculates

Significance

Spermatozoon swimming performance is critical for fertilization success in fishes, yet the cellular mechanisms that regulate this vital trait are poorly understood. Here, we discovered that a water channel protein, acting as an H_2O_2 channel (peroxiporin) to detoxify the mitochondria, directly regulates the velocity and progressive motility of both freshwater and marine spermatozoa. The mitochondrial insertion of the peroxiporin is controlled by an increasingly sophisticated hierarchy of intracellular signaling cascades, which evolved into a multiplier stress-activated pathway in modern marine species. These adaptive solutions maximize the postactivated swimming performance of sperm under conditions of high osmotic and oxidative stress. Our findings thus reveal that the pathways regulating the peroxiporin transport in fish spermatozoa provide an advantage for competitive fertilization success.

Author contributions: F.C. and J.C. designed research; F.C., C.D., A.F., and T.H. performed research; T.H., M.C., and J.A. contributed new reagents/analytic tools; F.C., R.N.F., and J.C. analyzed data; and F.C., R.N.F., and J.C. wrote the paper.

The authors declare no competing interest.

This article is a PNAS Direct Submission.

[1]To whom correspondence may be addressed. Email: joan.cerda@irta.cat.

This article contains supporting information online at https://www.pnas.org/lookup/suppl/doi:10.1073/pnas.2019346118/-/DCSupplemental.

Published March 4, 2021.

of freshwater (FW) and marine teleosts are not only rapidly diluted, but respectively face tremendous and opposing osmotic stresses, which in most species activate sperm motility (31–33). To understand the significance of such harsh environments for peroxiporin signal transduction pathway evolution, we selected model species from ancient and modern lineages of teleosts, including the FW ostariphysan zebrafish (*Danio rerio*), the FW protacanthopterygian Atlantic salmon (*Salmo salar*), and the modern marine acanthomorph gilthead seabream (*Sparus aurata*). Using a combination of pharmacological, molecular, and physiological approaches, we uncover the evolution of increasingly sophisticated peroxiporin signal transduction pathways powering their spermatozoa. The findings provide insight into the underlying hierarchy of systemic molecular traits that regulate the velocity, progressivity and duration of spermatozoon motility.

Results

Activated Piscine Spermatozoa Traffic the Aqp8bb Peroxiporin to Mitochondria. To investigate whether Aqp8bb is trafficked to the mitochondria of activated spermatozoa of FW teleosts as observed in the marine gilthead seabream (26), we first confirmed that the Aqp8bb orthologs of Atlantic salmon and zebrafish are expressed in intratesticular and ejaculated spermatozoa (*SI Appendix*, Figs. S1 and S2). Immunofluorescence microscopy of sperm maintained in the corresponding nonactivating medium (NAM), previously loaded with the mitochondrion-specific vital dye MitoTracker Red CMXRos (MTR), and using species-specific affinity-purified Aqp8bb antibodies, showed that the seabream Aqp8bb peroxiporin was distributed in the midpiece region and anterior part of the flagellum in immotile sperm, whereas in salmon and zebrafish Aqp8bb was mostly located in more discrete areas surrounding the spermatozoon head (Fig. 1 *A*–*C*). Upon SW- (seabream) or FW- (salmon and zebrafish) activation of sperm motility, Aqp8bb was rapidly accumulated in the mitochondria of each species (Fig. 1 *A*–*C*). Quantification of immotile and motile spermatozoa showing colocalization of Aqp8bb and MTR signals indicated that >75% of activated spermatozoa from each species showed Aqp8bb mitochondrial accumulation (Fig. 1 *D*–*F*), revealing that the peroxiporin trafficking mechanism during sperm motility is a conserved trait in teleosts.

Signaling Pathways Involved in Aqp8bb Intracellular Trafficking in SW Spermatozoa. To uncover the signaling pathways involved in the Aqp8bb trafficking mechanism of seabream spermatozoa, we used a battery of protein kinase inhibitors and activators (Fig. 2 and *SI Appendix*, Table S1). Immunofluorescence microscopy and immunoblotting data showed that the transit of Aqp8bb to the SW-activated sperm mitochondrion was strongly inhibited in a dose-dependent manner by the JNK inhibitor SP600125 with respect to spermatozoa treated with dimethyl sulfoxide (DMSO) vehicle (control), whereas CHIR99021 and BIM-II, typical blockers of glycogen synthase kinase 3 (GSK3) and protein kinase C (PKC), respectively, also reduced Aqp8bb transport but were less effective (Fig. 2 *A* and *B*). In contrast, inhibitors of p38 mitogen-activated protein kinase (p38 MAPK) and protein kinase A (PKA), such as SB202190 and BIRB796, and H-89, respectively, showed no effect (Fig. 2 *A* and *B*). We further tested the effect of inhibitors of several JNK upstream regulators, including the MAPKKKs MAP3K7/TAK1, germinal center kinases (GCKs), apoptosis signal-regulating kinase 1 (ASK1), and mitogen-activated protein kinase kinases (MKKs) (34), on Aqp8bb trafficking, using the compounds NG25, GNF-7, NQDI-1, and PD98059. The data indicated that only ASK1 and MKKs inhibitors can reduce Aqp8bb mitochondrial accumulation in a dose-dependent manner (Fig. 2 *A* and *B*), suggesting that a canonical ASK1-MKK-JNK cascade, as well as PKC and GSK3 signaling pathways, regulate Aqp8bb trafficking in activated seabream spermatozoa.

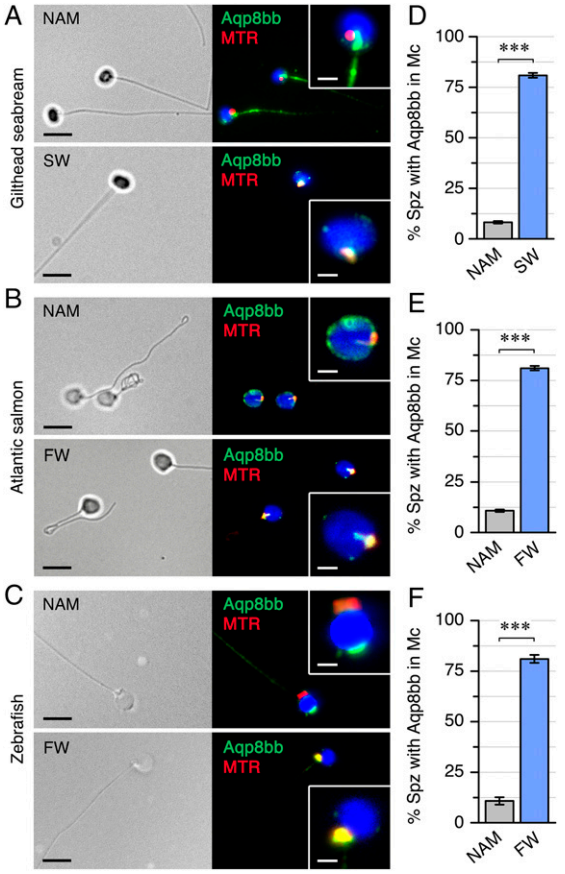

Fig. 1. The piscine Aqp8bb peroxiporin is transported to the mitochondria during spermatozoon motility activation. (*A*–*C*) Representative bright field images (*Left*) and immunodetection (*Right*) of Aqp8bb (green) in immotile (diluted in NAM) and activated spermatozoa of SW and FW spawning teleosts, using species-specific Aqp8bb antibodies. The mitochondria are labeled with MTR (red), whereas the spermatozoa nucleus are counterstained with DAPI (blue). Colocalized signals in mitochondria are yellow. (Scale bars, 5 μm; *Insets*, 1 μm.) (*D* and *F*) Percentage of spermatozoa showing Aqp8bb mitochondrial localization after incubation in NAM or upon activation in SW or FW in each species. Data are the mean ± SEM ($n = 4$ to 5 fish in *D* and *E*, and $n = 3$ pools of 5 different males each in *F*). Significance was measured by an unpaired Student's *t* test with respect to immotile sperm. ***$P < 0.001$.

Immunoblotting experiments confirmed the expression of ASK1, MKK4, JNK, and GSK3α/β kinases in immotile seabream spermatozoa (*SI Appendix*, Fig. S3*A*). Upon the hyperosmotic shock in SW, the phosphorylation of MKK4^{T261}, JNK$^{T183/Y185}$, and GSK3α/β$^{Y279/216}$ increased, whereas the inhibitory phosphorylation of ASK1^{S966} and GSK3α^{S21} decreased, suggesting that the catalytic activities of all of these kinases are activated (35–37). The inhibitory phosphorylation of GSK3β^{S9} seems not to be involved during seabream sperm activation, since phosphorylated GSK3β^{S9} was detected in testis extracts but not in spermatozoa (*SI Appendix*, Fig. S3*B*). Phosphorylation of JNK$^{T183/Y185}$ in SW-activated sperm was not affected by inhibitors of JNK, p38 MAPK, PKA, or GSK3 kinetic activity (Fig. 2*C*). However, JNK$^{T183/Y185}$ phosphorylation was reduced by PKC inhibition, although not completely, whereas that of Gsk3α/β$^{Y279/216}$ was partially decreased by both PKC and JNK blockage (Fig. 2*C*). Upon SW activation, the respective inhibition of the JNK upstream kinases ASK1 and MKK4 decreased MKK4^{T261}, JNK$^{T183/Y185}$, and GSK3α/β$^{Y279/216}$ phosphorylation (Fig. 2*C*), which is in accordance with the known role of ASK1 phosphorylating MKK4 (34) and the ability of PD98059 to prevent MKKs activation (38). Together, these data suggest that the ASK1-MKK4-JNK

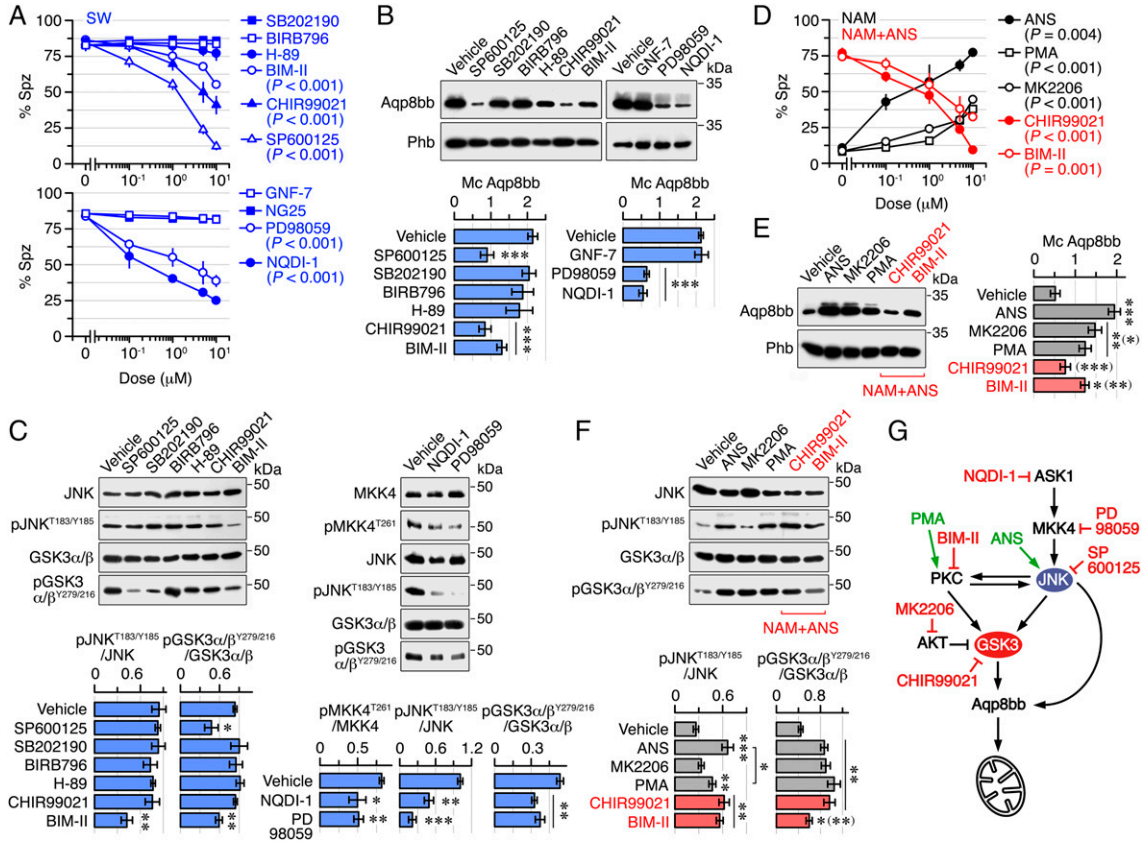

Fig. 2. Pharmacological identification of the major signal transduction pathways involved in Aqp8bb mitochondrial trafficking in seabream spermatozoa. (*A*) Dose–response inhibition of the percentage of activated spermatozoa showing Aqp8bb and MTR mitochondrial colocalization after treatment with DMSO alone (vehicle) or containing different protein kinase inhibitors determined by immunofluorescence microscopy. (*B*) Representative Aqp8bb immunoblots in mitochondrial extracts (*Upper*), and corresponding quantitation normalized to Phb (*Lower*), from sperm in *A* treated with 10 μM of the different drugs. (*C*) Total and phosphorylated JNK and GSK3 representative immunoblots (*Upper*) in sperm from *B*, and densitometric analysis of kinase phosphorylation normalized to the corresponding total kinase blot (*Lower*). (*D* and *E*) Activation of mitochondrial Aqp8bb trafficking in immotile spermatozoa maintained in NAM and exposed to activators of JNK (ANS), PKC (PMA), or GSK3 (MK2206) (black color) determined by immunofluorescence microscopy (*D*) and immunoblotting (*E*). Inhibition of ANS (10 μM)-induced Aqp8bb transport by inhibitors of GSK3 (CHIR99021) and PKC (BIM-II) is shown in red color. (*F*) MKK4, JNK, and GSK3 activation in sperm treated as in *D*. (*G*) Proposed model of the JNK and GSK3 signaling pathways controlling Aqp8bb mitochondrial transport in activated seabream spermatozoa. The kinase inhibitors (red color) and activators (green color) used are indicated. In *A*–*F*, data (mean ± SEM; $n = 3$ to 7 fish) were statistically analyzed by one-way ANOVA (*P* values for each compound are indicated in *A* and *D*). ***$P < 0.001$; **$P < 0.01$; *$P < 0.05$, with respect to control spermatozoa (treated with DMSO vehicle) or as indicated in brackets, or with respect to sperm treated with ANS alone (*E* and *F* in parenthesis).

cascade can partially activate GSK3, and that PKC activity is required for full JNK and GSK3 activation. This combination can explain the somewhat lower potency of PKC inhibition to prevent Aqp8bb mitochondrial transport. However, the strong reduction of Aqp8bb trafficking by JNK inhibition suggests an additional role of JNK on channel trafficking that is not mediated by GSK3.

In order to assess the potential interaction of the JNK, PKC, and GSK3 pathways in the regulation of Aqp8bb mitochondrial transport, we investigated whether this mechanism could be stimulated in immotile spermatozoa. For this, NAM-maintained sperm were treated with the JNK/p38 MAPK phosphorylation-inducer anisomycin (ANS) and the PKC analog activator phorbol 12-myristate 13-acetate (PMA), as well as with MK2206 and SH-5, which are AKT/PKB inhibitors that can indirectly activate GSK3 (39, 40). The data show that all of these drugs stimulated Aqp8bb mitochondrial trafficking, while treatment with the PKC inactive enantiomer 4α-PMA had no effect (Fig. 2 *D* and *E* and *SI Appendix*, Fig. S4*A*). However, the percentage of spermatozoa showing Aqp8bb localization in the mitochondrion after exposure to ANS was similar to that observed in SW-activated sperm, whereas the other compounds only promoted channel mitochondrial accumulation in approximately half of the cells (Fig. 2 *D* and *E* and *SI Appendix*, Fig. S4*A*). The stimulatory effect of ANS on Aqp8bb trafficking, which occurs through JNK and not p38 MAPK (*SI Appendix*, Fig. S4 *B* and *C*), was completely blocked by GSK3 inhibition, but only partially reduced by the PKC inhibitors BIM-II and calphostin C (Fig. 2 *D* and *E* and *SI Appendix*, Fig. S4*A*). This suggests that PKC activation by JNK is necessary to drive Aqp8bb mitochondrial transport, but that this mechanism can still be triggered to some extent by JNK independently of PKC. The positive effects of PMA and MK2206 on Aqp8bb transport were not additive and could be reduced by JNK and GSK3 inhibition (*SI Appendix*, Fig. S4 *D* and *E*), suggesting that PKC and GSK3 activate the same mechanism for Aqp8bb trafficking, with both kinases dependent on active JNK.

Activation of JNK and PKC by ANS and PMA treatments, respectively, in immotile spermatozoa induced the phosphorylation of $JNK^{T183/Y185}$ and $GSK3\alpha/\beta^{Y279/216}$, thus supporting that JNK and GSK3 can be activated via PKC, and that activation of GSK3 by JNK occurs during Aqp8bb trafficking (Fig. 2*F*). In contrast, MK2206 activated GSK3 but not JNK, indicating that GSK3 is downstream of JNK (Fig. 2*F*). However, as noted earlier, active JNK was still necessary for MK2206-induced Aqp8bb transport, thus supporting a role of JNK regulating mitochondrial

Aqp8bb transport independently of GSK3. The ANS-mediated $JNK^{T183/Y185}$ phoshorylation was not affected by PKC or GSK3 inhibition, while that of GSK3α/$β^{Y279/216}$ was moderately reduced by PKC inhibition but it was not affected by the GSK3 blocker (Fig. 2*F*). Therefore, this also confirms that JNK can partially activate GSK3 in the absence of PKC activation.

Taken together, our findings suggest that a cross-talk between the PKC and JNK signaling pathways triggers the GSK3-mediated trafficking of the Aqp8bb peroxiporin to the inner mitochondrial membrane of the seabream spermatozoon (Fig. 2*G*). Moreover, a direct additive action of JNK, which bypasses the GSK3 pathway, acts as a multiplier for the rapid trafficking mechanism (Fig. 2*G*).

GSK3 and JNK Control Aqp8bb-Mediated Mitochondrial Detoxification in Activated Seabream Spermatozoa. Since JNK and GSK3 appear to be key regulators of Aqp8bb trafficking, we investigated whether the pharmacological blockage of their activities can impair Aqp8bb insertion into the spermatozoon inner mitochondrial membrane and hamper H_2O_2 efflux. An Aqp8bb immunoblot of inner membrane mitochondrial extracts from SW-activated spermatozoa confirmed that the amount of mitochondrial Aqp8bb was lower in sperm treated with the JNK and GSK3 inhibitors compared to controls (Fig. 3*A*). The low mitochondrial abundance of Aqp8bb in these groups was associated with a reduced ability of mitochondria to transport H_2O_2 as measured with the ROS-sensitive, cell permeable fluorescent dye 5-(and -6)-chloromethyl-2′,7′-dichlorodihydrofluorescein diacetate, acetyl ester (CM-H_2DCFDA) (Fig. 3*B*). As a consequence, a higher accumulation of H_2O_2 in the spermatozoa exposed to the JNK and GSK3 inhibitors with respect to controls was observed during activation (Fig. 3*C*). The increased intracellular ROS was harmful to sperm function since time-course monitoring of sperm motion kinetics using computer-assisted sperm analysis (CASA) for up to 180 s revealed that both inhibitors reduced the percentage of motility and progressivity of the spermatozoa, as well as their curvilinear velocity (VCL), with respect to sperm treated with DMSO alone (Fig. 3*D*). However, the three sperm motion parameters measured within the first 30 s postactivation were more diminished when the JNK pathway is blocked (17 ± 1% and 35 ± 5% inhibition with the GSK3 and JNK blockers, respectively, with respect to the controls; $n = 9$, $P = 0.003$, Student's t test). The addition of the mitochondria-targeted antioxidant Mito-TEMPO recovered sperm motion kinetics within 60 to 70 s, except there was reduction in the percentage of motile spermatozoa induced by GSK inhibition (Fig. 3*E*). This suggests that GSK3 likely plays other roles to maintain sperm motility in addition to mitochondrial Aqp8bb trafficking. These observations are thus consistent with a role of the JNK and GSK3 signaling pathways regulating Aqp8bb mitochondrial detoxification and the kinematic properties of the spermatozoa.

Intracellular Ca^{2+} and ROS Trigger Seabream Aqp8bb Mitochondrial Transport. We previously demonstrated that prevention of the intracellular Ca^{2+} surge that normally occurs in seabream sperm upon SW activation partially inhibits mitochondrial Aqp8bb trafficking (41), and that the SW-induced hyperosmotic shock increases ROS levels in the spermatozoa (26). Since it is known that the ASK1-MAPK signaling pathway can be activated by cellular oxidative stress (42), we hypothesize that elevated intracellular concentrations of Ca^{2+} ($[Ca^{2+}]_i$) and ROS linked to the hyperosmotic shock in SW are the upstream signals in seabream spermatozoa triggering JNK and GSK3 activation and Aqp8bb intracellular trafficking.

To investigate this hypothesis, we first determined the contribution of Ca^{2+}-activated signaling pathways in the regulation of Aqp8bb mitochondrial transport by treating immotile sperm with 3 mM Ca^{2+} in the presence of 10 μM of the Ca^{2+} ionophore A23187, which generates similar levels of $[Ca^{2+}]_i$ to those determined in SW-activated sperm (Fig. 4*A*). Under these conditions, Aqp8bb transport to the mitochondria was enhanced, but interestingly, the percentage of spermatozoa showing mitochondrial localization of the channel was approximately half of that observed in SW-activated sperm (Fig. 4*B*). Ca^{2+}-triggered Aqp8bb trafficking was not affected by inhibitors of ASK1 and MKK, whereas it was reduced to control levels by blockers of PKC, JNK, and GSK3 (Fig. 4*C* and *SI Appendix*, Fig. S5). After Ca^{2+} treatment, the inhibitory phosphorylation of $ASK1^{S966}$ did not change, and MKK4 was not activated, while phosphorylation of $JNK^{T183/Y185}$ and GSK3α/$β^{Y279/216}$ was enhanced (Fig. 4*D*). The activation of JNK and GSK3 was reduced by PKC inhibition, while the blockage of JNK only partially diminished GSK3 activation (Fig. 4*D*). These data suggest that a $[Ca^{2+}]_i$ surge alone can partially trigger JNK- and GSK3-mediated Aqp8bb mitochondrial transport through PKC activation of JNK and GSK3, and thus independently of the ASK1-MKK4 signaling pathway.

To examine the effect of oxidative stress on Aqp8bb intracellular trafficking in spermatozoa, independently of the Ca^{2+} signal, we followed two different approaches: The generation of ROS in immotile sperm by exposure to the xanthine-xanthine oxidase (X-XO) system (43), and the treatment of SW-activated sperm with the Ca^{2+} chelator 1,2-bis(2-aminophenoxy)ethane-N,N,N′,N′-tetraacetic acid (BAPTA) in the presence or absence of diphenyleneiodonium (DPI), a compound that limits ROS production by inhibiting membrane-bound NADPH oxidases (NOXes) and other flavoproteins (44). External treatment of nonactivated sperm with X-XO produced an increment of ROS in a dose–response manner, the highest X-XO dose generating similar ROS levels to those measured in SW-activated sperm (Fig. 5 *A* and *D*). Upon SW activation, treatment with BAPTA abolished the $[Ca^{2+}]_i$ surge in a dose-dependent manner, which completely inhibited motility (*SI Appendix*, Fig. S6*A*), while ROS accumulation in the spermatozoa was not affected (Fig. 5 *B* and *D*). Conversely, exposure of activated sperm to DPI decreased ROS levels but did not affect the increase of $[Ca^{2+}]_i$ (Fig. 5 *C* and *D*). Interestingly, as previously observed in Ca^{2+}-treated immotile sperm, treatment of immotile spermatozoa with the highest dose of X-XO stimulated Aqp8bb mitochondrial trafficking in approximately half of the spermatozoa with respect to SW-activated sperm exposed to DMSO alone (*SI Appendix*, Fig. S6*B*). The same result was observed in sperm activated in SW containing BAPTA (*SI Appendix*, Fig. S6*C*).

In both ROS- and SW+BAPTA-treated spermatozoa, Aqp8bb mitochondrial accumulation was completely inhibited by blockers of ASK1, MKK, JNK, and GSK3, whereas inhibition of PKC only partially decreased Aqp8bb transport (Fig. 5*E* and *SI Appendix*, Fig. S6 *B–D*). The ROS generated in immotile and SW spermatozoa activated ASK1 by deposphosphorylation of the inhibitory $ASK1^{S966}$ site, which was not affected by any of the downstream kinase inhibitors, while it enhanced the phosphorylation of $MKK4^{T261}$, $JNK^{T183/Y185}$, and GSK3α/$β^{Y279/216}$ (Fig. 5*F* and *SI Appendix*, Fig. S6*E*). Activation of MKK4 was reduced to control levels by inhibitors of ASK1 and MKK, but not by inhibition of downstream kinases, whereas ROS-induced JNK and GSK3 activation was completely blocked by ASK1 and MKK inhibitors, and only partially prevented by PKC inhibition (Fig. 5*F* and *SI Appendix*, Fig. S6*E*). However, JNK inhibition strongly reduced ROS-mediated GSK3 activation (Fig. 5*F* and *SI Appendix*, Fig. S6*E*), which indicates that the ROS-triggered ASK1-MKK4-JNK pathway can activate GSK3 independently of PKC. The data, however, also suggest that ROS-induced PKC activity may be a positive regulator of JNK, as previously observed after Ca^{2+} treatment alone, but that in this case this mechanism requires previous activation of JNK by the canonical upstream kinase MKK4.

Consistent with this model, when either the $[Ca^{2+}]_i$ or ROS increments in SW-activated sperm were completely abolished by BAPTA and DPI, respectively, the percentage of spermatozoa showing mitochondrial localization was similar to that elicited by

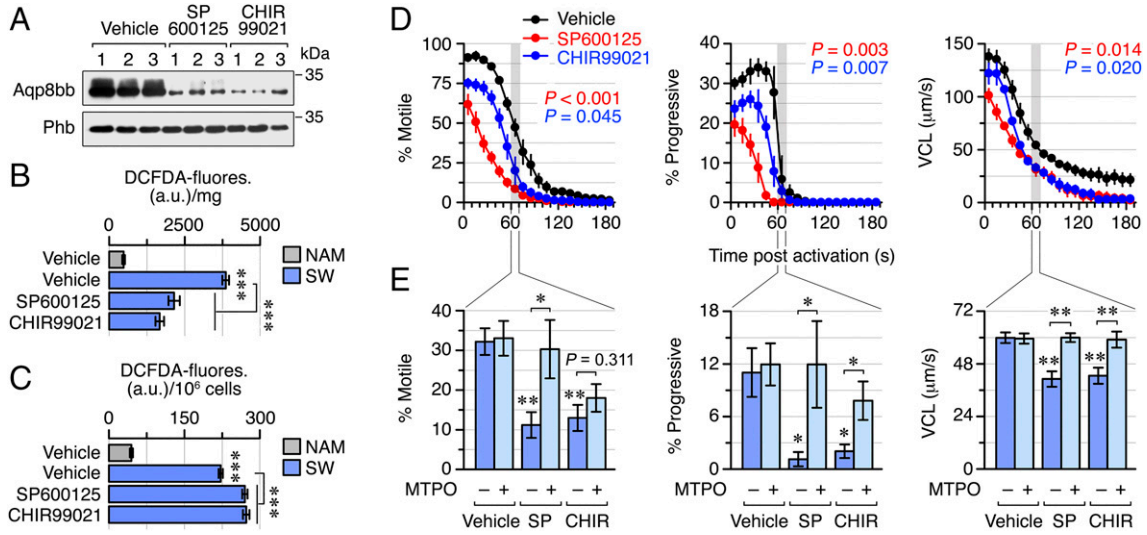

Fig. 3. JNK and GSK3 inhibition prevents Aqp8bb insertion into the seabream spermatozoa inner mitochondrial membrane upon SW activation. (*A*) Aqp8bb immunoblot in the inner mitochondrial membrane from SW-activated spermatozoa ($n = 3$ fish) exposed or not to 10 μM of the JNK (SP600125) and GSK3 (CHIR99021) inhibitors. Phb was used as a marker for even loading. (*B*) H_2O_2 uptake (mean ± SEM, $n = 6$ fish) by mitochondria isolated from NAM and SW spermatozoa treated with or without the inhibitors. (*C*) ROS levels (mean ± SEM, $n = 8$ fish) in spermatozoa treated as in *B*. Statistical differences were measured by one-way ANOVA. ***$P < 0.001$, with respect to NAM or SW-activated sperm not treated with the inhibitors, or as indicated in brackets. (*D*) Percentage of motility and progressivity, and VCL, of spermatozoa (mean ± SEM, $n = 4$ fish) treated with DMSO in the presence or absence of SP600125 and CHIR99021. Statistical differences with respect to control spermatozoa (only during the first 60 s for motility and progressivity) were determined by the Mann–Whitney *U* test (*P* values indicated in each panel). (*E*) Effect of the mitochondria-targeted antioxidant Mito-TEMPO (MTPO; 50 μM) on the SP600125 (SP) or CHIR99021 (CHIR) inhibition of sperm kinetics (mean ± SEM, $n = 7$ fish) at 60 to 70 s postactivation (marked with a gray bar in *D*). Data are statistically analyzed by one-way ANOVA (minus MTPO), and by the unpaired Student's *t* test between sperm untreated and treated with MTPO. *$P < 0.05$; **$P < 0.01$; ***$P < 0.001$, with respect to nontreated sperm, or as indicated in brackets.

ROS treatment of immotile spermatozoa, and was approximately half of that observed in SW-activated sperm (Fig. 5 *G* and *H*). However, when both inhibitors were present upon SW activation, Aqp8bb mitochondrial accumulation was strongly reduced to the level observed in immotile spermatozoa (Fig. 5 *G* and *H*). Kinase phosphorylation analysis showed that while ASK1 activation in SW-activated spermatozoa was not affected by BAPTA treatment, DPI reduced both ASK1 and MKK4 activation (Fig. 5*I*). In contrast, each of the BAPTA and DPI treatments only partially prevented JNK and GSK3 activation (Fig. 5*I*). In the presence of BAPTA plus DPI, the activation state of ASK1 and MKK4 did not change with respect to that observed in the presence of DPI alone, whereas the activation of JNK and GSK3 was strongly diminished (Fig. 5*I*).

Taken together, these findings suggest that the intracellular Ca^{2+} and ROS signals occurring in SW-activated seabream spermatozoa respectively trigger alternative and additive PKC and ASK1-MAPK pathways, which cross-talk to activate JNK and GSK3 and direct Aqp8bb mitochondrial insertion.

JNK and GSK3 Can Phosphorylate Seabream Aqp8bb In Vitro. In silico analysis of the seabream Aqp8bb amino acid sequence revealed the presence of three Ser residues (Ser^{16}, Ser^{19}, and Ser^{20}) and one Thr (Thr^{24}) residue in the N terminus of the channel as potential phosphorylation recognition sites for GSK3 and proline-directed kinase (such as p38 MAPK and JNK), respectively (*SI Appendix*, Fig. S7*A*). An additional Ser residue (Ser^{91}) showing a low score for GSK3 and proline-directed kinase phosphorylation was also identified in the first cytoplasmic loop (*SI Appendix*, Fig. S7*A*). To experimentally assess whether GSK3 and JNK can phosphorylate seabream Aqp8bb, we employed in vitro phosphorylation assays using mouse recombinant JNK1 (rJNK1) and human recombinant GSK3β (rGSK3). In these experiments, Flag-tagged Aqp8bb (Aqp8bb-Flag) transiently expressed in embryonic kidney cells 293T (HEK293T) was immunoprecipitated using the seabream Aqp8bb specific antibody and incubated with rJNK1 or rGSK3β in the presence or absence of ATP. Immunobloting of immunoprecipitated Aqp8bb-Flag using phosphorylated Ser- and Thr-specific antibodies confirmed the ATP-dependent specific phosphorylation of Aqp8bb Ser and Thr residues by rJNK1, and only of Ser residues by rGSK3β (*SI Appendix*, Fig. S7*B*). To determine which specific channel residues are phosphorylated by the kinases, the same assays were carried out using wild-type Aqp8bb-Flag (Aqp8bb-Flag-WT) or Aqp8bb-Flag constructs in which all Ser and Thr residues in the N terminus, as well as Ser^{91}, were independently mutated into Ala. The results showed that Aqp8bb-Flag-T24A and -S91A prevented rJNK1 Thr and Ser phosphorylation, respectively, whereas Aqp8bb-Flag-S16A abolished Ser phosphorylation by rGSK3β (*SI Appendix*, Fig. S7*C*). These data therefore indicate that Thr^{24} and Ser^{91} are the residues phosphorylated by rJNK1, while only Ser^{16} is the target site for rGSK3β.

The majority of GSK3 substrates require prephosphorylation at a residue 4 or 5 amino acids C-terminal to the GSK3 target site for full catalytic activity, a phenomenon referred to as "priming" (45). The seabream Aqp8bb shows two such potential priming sites, Ser^{19} and Ser^{20}, located three and four residues C-terminal to the Ser^{16} GSK3 phosphorylation site (*SI Appendix*, Fig. S7*A*). In addition, Thr^{24} could also play a role since some substrates of GSK3 show a priming site much further from the target site (45). To investigate whether a priming mechanism regulates rGSK3β-mediated Aqp8bb phosphorylation at Ser^{16}, we first established by immunoblotting the lowest amount of rGSK3β to yield detectable levels of Ser phosphorylation in Aqp8bb (*SI Appendix*, Fig. S7*D*), and subsequently test if Aqp8bb-Flag-S19D, -S20D, and -T24D mutants, which mimic a phosphorylated state, increase rGSK3β-mediated channel phosphorylation. The results show that Ser^{16} phosphorylation of Aqp8bb-Flag by rGSK3β was increased by ~27 times in Aqp8bb-Flag-S19D and -S20D mutants with respect to the wild-type, whereas the Aqp8bb-Flag-T24D was phosphorylated

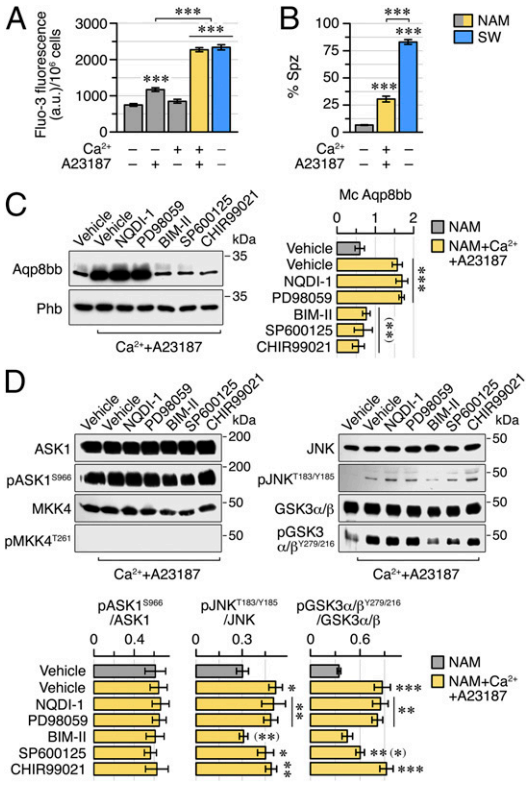

Fig. 4. An intracellular Ca^{2+} surge partially drives Aqp8bb transport to the mitochondrion in nonactivated seabream spermatozoa. (*A*) Intracellular Ca^{2+} levels in sperm maintained in NAM and treated with 3 mM Ca^{2+} and/or 10 μM of the Ca^{2+} ionophore A23187, and in SW-activated sperm. (*B*) Percentage of spermatozoa showing Aqp8bb mitochondrial localization after exposure to Ca^{2+} and A23187 in NAM, or upon activation in SW. (*C*) Representative immunoblot of mitochondrial Aqp8bb (*Left*), and corresponding quantitation normalized to Phb (*Right*), from sperm incubated with or without Ca^{2+} and A23187 in NAM, and treated with 10 μM of different kinase inhibitors. (*D*) Total and phosphorylated ASK1, MKK4, JNK, and GSK3α/β representative immunoblots (*Upper*) in spermatozoa treated as in *C*. (*Lower*) Depiction of the densitometric analysis of kinase phosphorylation normalized to the corresponding band from the total kinase blot. Data are the mean ± SEM (n = 4 to 6 fish) and are statistically analyzed by one-way ANOVA. ***$P < 0.001$; **$P < 0.01$; *$P < 0.05$, with respect to nontreated sperm, or treated with Ca^{2+}+A23187 without inhibitors (in parenthesis), or as indicated in brackets.

at Ser^{16} ~12 times more efficiently (*SI Appendix*, Fig. S7*E*). These findings therefore suggest that Aqp8bb phosphorylation of Ser^{19}, Ser^{20}, and to a lesser extent Thr^{24}, can prime the channel N terminus for Ser^{16} phosphorylation by GSK3 (*SI Appendix*, Fig. S7*F*).

GSK3 and JNK Phosphorylation of Ser^{16} and Thr^{24}, Respectively, in Seabream Aqp8bb Regulate Channel Trafficking. Transcriptional and translational activity in ejaculated sperm is very low or completely absent (46). Therefore, in order to investigate the molecular basis of Aqp8bb mitochondrial trafficking, we examined whether the signaling pathways controlling this mechanism in spermatozoa can be reproduced in cultured mammalian cells. For these tests, we selected the human hepatocarcinoma-derived cell line HepG2 in which the AQP8 ortholog is expressed in the inner mitochondrial membrane (47). The results of these experiments showed that the same Ca^{2+}-activated PKC-GSK3 and H_2O_2-activated JNK-GSK3 signaling cascades controlling Aqp8bb mitochondrial transport in the seabream spermatozoon can be replicated in HepG2 cells, except that in this case the cross-talk between PKC and JNK does not occur (*SI Appendix*, *Supplementary Text S1* and Fig. S8).

Using the HepG2 cells as a surrogate system for functional analyses, we investigated the role of Aqp8bb phosphorylation on mitochondrial channel trafficking. To this end, we transfected cells with Aqp8bb-Flag-WT or single phosphomimetic mutants at each Ser and Thr residue in the N terminus of the channel (Aqp8bb-Flag-T2D, -T15D, -S16D, -S19D, -S20D, -T24D), and at Ser^{91} (Aqp8bb-Flag-S91D), or with a S16D/T24D double mutant, and subsequently determined mitochondrial targeting of the encoded proteins by immunofluorescence microscopy. The data showed that Aqp8bb-Flag-WT and the Aqp8bb-Flag-S91D mutant mainly remained in the cell plasma membrane, whereas the Aqp8bb-Flag-T2D and -T15D channels were retained in the cytoplasm (Fig. 6*A* and *SI Appendix*, Fig. S9*A*). In contrast, the Aqp8bb-Flag-S19D and -S20D mutants were partially targeted to the mitochondria, which appears to be enhanced for the Aqp8bb-Flag-S16D, -T24D and S16D/T24D channel constructs (Fig. 6*A*). Immunoblot analysis showed that the wild-type and mutant channels were expressed at similar levels, and confirmed that each of the Aqp8bb-Flag-S16D and -T24D mutants were targeted to the mitochondria, unlike the Aqp8bb-Flag-WT (Fig. 6*B*). The Aqp8bb-Flag-S19D and -S20D constructs also accumulated in the mitochondria but to a lesser amount than the Aqp8bb-Flag-S16D and -T24D mutants (Fig. 6*B*). However, the data also revealed that the Aqp8bb-Flag-S16D/T24D double mutant was more concentrated in the mitochondria than each of the corresponding single mutants (Fig. 6*B*), suggesting that phosphorylation of Ser^{16} and Thr^{24} residues in the channel are additive for activating mitochondrial transport.

To further investigate the role of Ser^{16} and Thr^{24} phosphorylation driving Aqp8bb mitochondrial trafficking, cells were transfected with Aqp8bb-Flag-WT or mutant channels in which one or both Ser^{16} and Thr^{24} were mutated into Cys or Ala, respectively, and treated with 10 mM Ca^{2+} and 100 μM H_2O_2. Immunoblot analyses of total protein extracts showed that the three Aqp8bb-Flag-S16C, -T24A, and -S16C/T24A mutants were equally expressed than the Aqp8bb-Flag-WT (*SI Appendix*, Fig. S9*B*). However, mitochondrial trafficking in response to Ca^{2+} and H_2O_2 treatment was similarly reduced in both Aqp8bb-Flag-S16C and -T24A constructs with respect to that shown by the Aqp8bb-Flag-WT, whereas channel transport of the Aqp8bb-Flag-S16C/T24A double mutant was almost completely abolished (Fig. 6*C*). Immunoprecipitation followed by immunoblot analysis of phosphorylated Ser and Thr showed that Aqp8bb-Flag-WT was phosphorylated at Ser and Thr residues in response to Ca^{2+} and H_2O_2 uptake (Fig. 6*C*). However, only Ser or Thr phosphorylation was reduced in the Aqp8bb-Flag-S16C and -T24A constructs, respectively, with respect to that seen in the Aqp8bb-Flag-WT, while phosphorylation of both Ser and Thr residues was decreased in the Aqp8bb-Flag-S16C/T24A double mutant (Fig. 6*C*). These data therefore support that Ser^{16} and Thr^{24} phosphorylation in the Aqp8bb N terminus are both necessary for maximum mitochondrial channel transport.

To confirm that GSK3 and JNK are, respectively, involved in Ser^{16} and Thr^{24} phosphorylation of Aqp8bb, HepG2 cells were cotransfected with Aqp8bb-Flag-WT and dominant-negative catalytically inactive forms of *Xenopus laevis* GSK3β (dnGSK3β) (48) or human JNK1 (dnJNK1) (49), and exposed to external Ca^{+2} and H_2O_2. Both inhibitory constructs reduced the accumulation of Aqp8bb-Flag-WT in the mitochondria in response to external Ca^{2+} and ROS (Fig. 6*D*), thus further supporting the role of JNK and GSK3 in the Aqp8bb trafficking mechanism. However, while dnGSK3β expression decreased Ser phosphorylation of Aqp8bb-Flag-WT, but not Thr phosphorylation, the dnJNK1 construct completely abolished Ser and Thr phosphorylation of the channel (Fig. 6*D*). These findings suggest that JNK could activate GSK3 for Aqp8bb Ser phosphorylation, in addition to its potential role

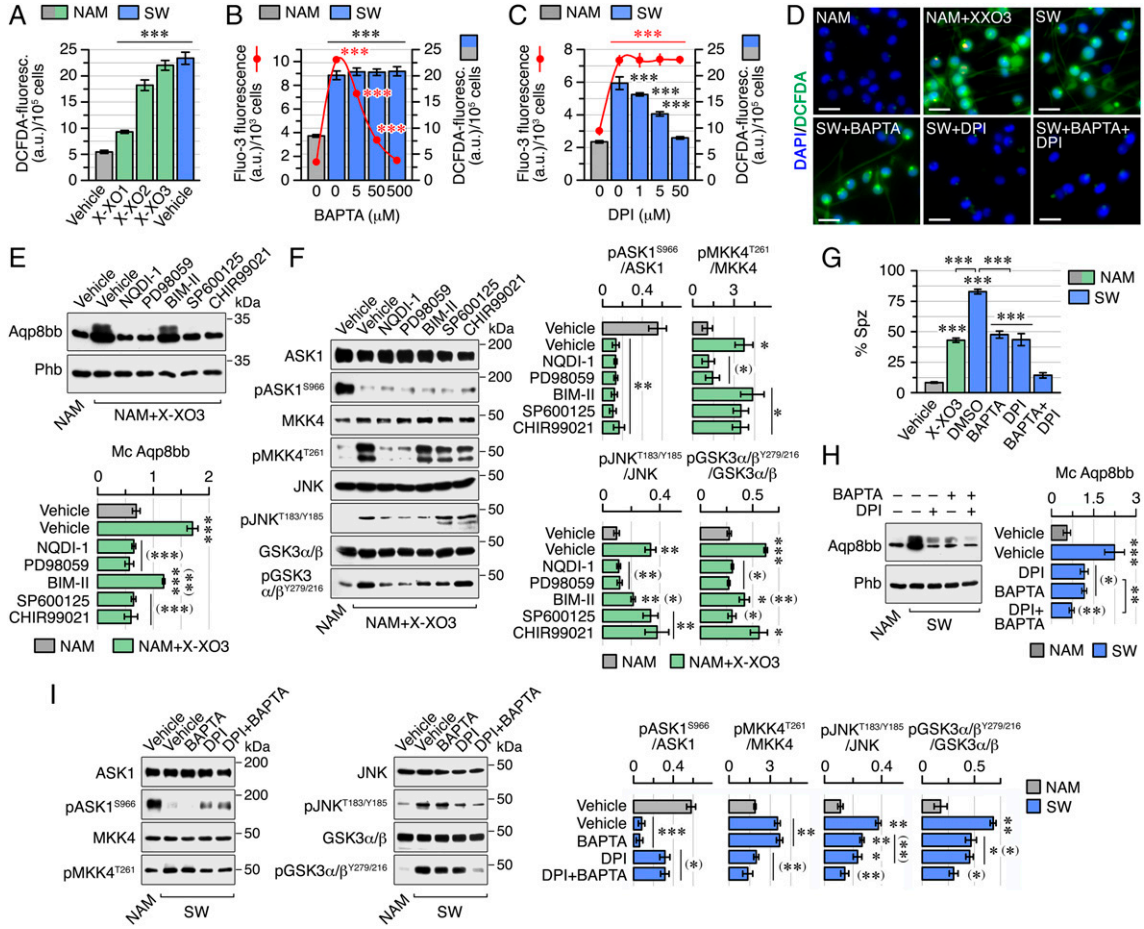

Fig. 5. Oxidative stress-induced Aqp8bb mitochondrial transport in seabream spermatozoa. (*A*) ROS levels in immotile sperm treated with increasing doses of X-XO (X-XO1, X-XO2, and X-XO3), and in SW-activated spermatozoa. (*B* and *C*) Intracellular Ca^{2+} (red line) and ROS levels (bars) in nonactivated and activated sperm in the presence of BAPTA (*B*) or DPI (*C*). (*D*) Epifluorescence photomicrographs of nonactivated and activated spermatozoa treated with X-XO3, 500 μM BAPTA, 50 μM DPI, or BAPTA+DPI, and labeled with the CM-H_2DCFDA dye (green). Nuclei are counterstained with DAPI (blue). (Scale bars, 5 μm.) (*E*) Immunoblot of mitochondrial Aqp8bb in sperm maintained in NAM and exposed to X-XO3 (*Upper*), in the presence or absence of 10 μM of kinase inhibitors, and corresponding quantitation normalized to Phb (*Lower*). (*F*) Total and phosphorylated ASK1, MKK4, JNK, and GSK3α/β immunoblots (*Left*), and densitometric analysis of phosphorylated forms normalized to the corresponding nonphosphorylated bands (*Right*), in spermatozoa treated as in *E*. (*G*) Percentage of spermatozoa showing Aqp8bb in mitochondria after treatment with X-XO3 in NAM, or upon activation in SW with or without BAPTA and/or DPI. (*H*) Immunoblot of mitochondrial Aqp8bb in immotile sperm or activated in SW with or without BAPTA and/or DPI (*Left*) and quantitation normalized to Phb (*Right*). (*I*) Immunoblots of kinase activation in sperm treated as in *H* (*Left*) and quantitation of phosphorylated forms. In all panels, data are displayed as mean ± SEM ($n = 4$ to 6 fish) and are statistically analyzed by one-way ANOVA. ***$P < 0.001$; **$P < 0.01$; *$P < 0.05$, with respect to nontreated spermatozoa in NAM, spermatozoa exposed to NAM plus X-XO3 or SW without inhibitors (in parenthesis), or as indicated in brackets (*G* and *E*).

phosphorylating Thr^{24} in the channel, as previously predicted to occur in sperm cells. To corroborate this hypothesis, activation of GSK3 was evaluated in HepG2 cells expressing Aqp8bb-Flag-WT and dnJNK1 and treated with Ca^{2+} and H_2O_2. The data confirmed that phosphorylation of GSK3α/$\beta^{Y279/216}$ was reduced in the presence of catalytically inactive JNK1, whereas that of GSK3α^{S21}, but not of GSK3β^{S9}, was increased (Fig. 6*E*). These results therefore suggest that mitochondrial trafficking of seabream Aqp8bb is regulated by Ser^{16} phosphorylation by JNK- and PKC-activated GSK3, as well as by JNK-mediated Thr^{24} phosphorylation of the channel.

Aqp8bb Mitochondrial Transport in FW Spermatozoa Is Controlled by PKC or GSK3 Phosphorylation of an N-Terminal Ser Residue. To examine whether the same signaling pathways regulating seabream Aqp8bb mitochondrial transport are present in FW spermatozoa, we initially assessed the effect of PKC, JNK, and GSK3 inhibitors (BIM-II, SP600125, and CHIR99021, respectively) on Aqp8bb trafficking in Atlantic salmon and zebrafish spermatozoa upon FW activation. In contrast to the seabream, the results showed that JNK inhibition did not affect mitochondrial channel transport in salmon and zebrafish sperm, indicating that the JNK signaling pathway is not involved in this mechanism (Fig. 7*A*). In contrast, both PKC and GSK3 inhibitors reduced the percentage of salmon spermatozoa showing Aqp8bb mitochondrial localization in a dose–response manner, whereas only the blockage of PKC elicited the same effect in zebrafish (Fig. 7*A*). These observations suggest a role of PKC and GSK3, and of PKC only, in the control of Aqp8bb transport in salmon and zebrafish spermatozoa, respectively.

To confirm that PKC is the signaling kinase controlling Aqp8bb-mediated mitochondrial detoxification in zebrafish spermatozoa, the levels of ROS in immotile and FW-activated sperm in the presence or absence of the PKC inhibitor BIM-II were determined. The results showed that the hypoosmotic shock in FW does not increase ROS levels in zebrafish sperm; however, when the transport of Aqp8bb to the mitochondria was impaired by PKC inhibition, ROS levels were increased (Fig. 7*B*). This reveals that an osmotic shock-induced ROS-MAPK-JNK signaling pathway

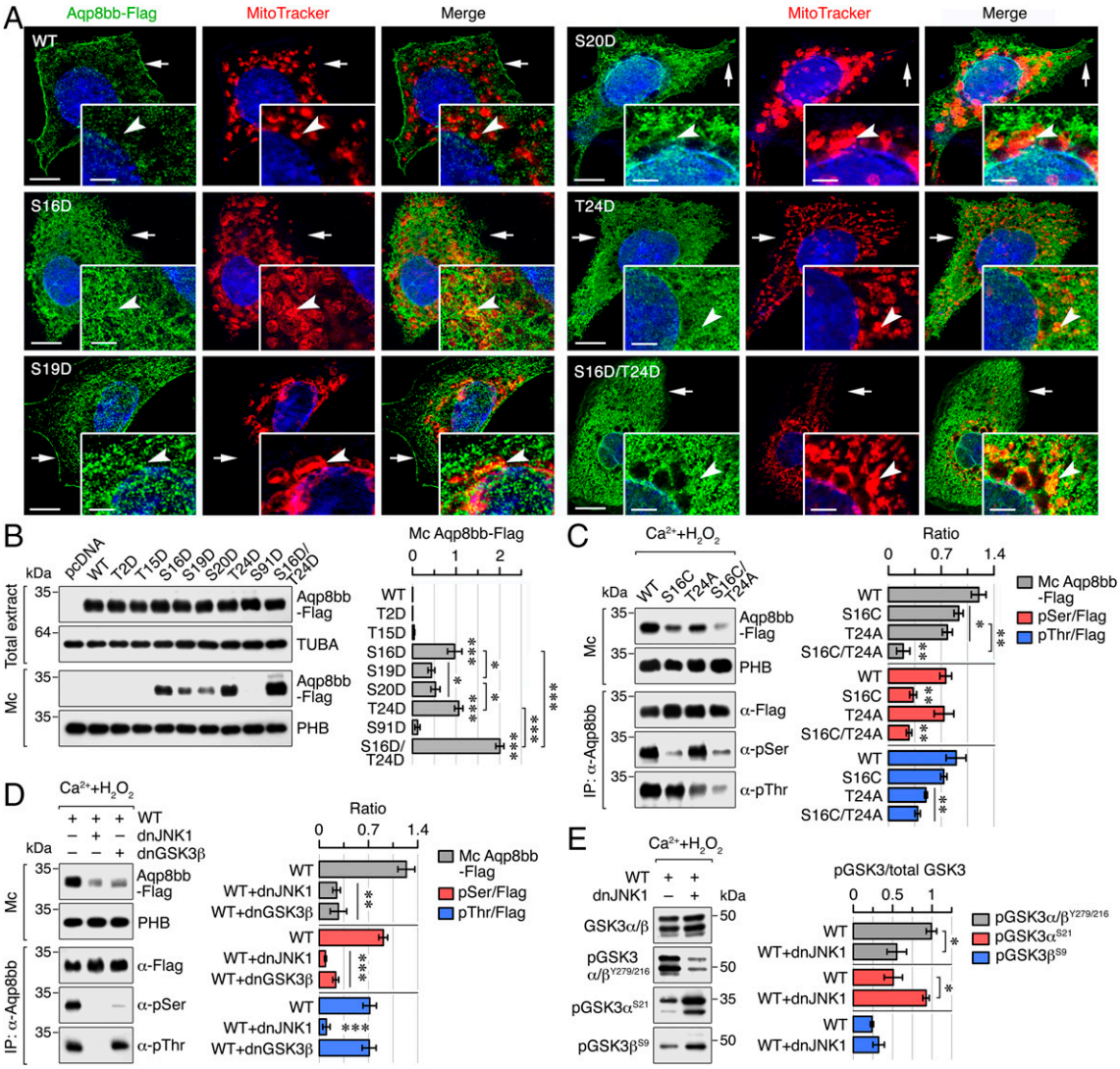

Fig. 6. Dual N terminus phosphorylation of seabream Aqp8bb by GSK3 and JNK control mitochondrial channel transport in HepG2 cells. (*A*) Double staining of Aqp8bb-Flag (green) and mitochondria (MTR, red) in cells transiently expressing wild-type Aqp8bb-Flag (WT) or phospho-mimetic mutants as indicated. Arrows point to the plasma membrane, whereas arrowheads indicate colocalized signals in the mitochondria. (Scale bars, 10 μm; *Insets*, 5 μm.) (*B*) Representative immunoblot of total and mitochondrial Aqp8bb-Flag-WT and mutants, using tubulin (TUBA) and PHB as loading controls, respectively (*Left*). Mitochondrial Aqp8bb-Flag quantitation is normalized to PHB (*Right*). (*C*) Immunoblot of mitochondrial Aqp8bb-Flag-WT and -S16C, -T24A, and -S16C/T24A mutant channels, and Ser and Thr phosphorylation of the corresponding immunoprecipitated proteins, in cells treated with Ca^{2+} and H_2O_2. (*Right*) The amount of each construct in the the mitochondria, normalized to PHB, and their Ser and Thr phosphorylation state normalized to the total immunoprecipitated protein. (*D*) Effect of coexpression of Aqp8bb-Flag-WT and dominant-negative forms of JNK1 and GSK3β (dnJNK1 and dnGSK3β, respectively) on the mitochondrial transport and Ser/Thr phosphorylation of the channel in cells treated as in *C*. (*E*) Immunoblot of nonactivated and activated GSK3 in cells coexpressing Aqp8bb-Flag-WT and dnJNK1 and treated with Ca^{2+} and H_2O_2 (*Left*), and densitometric analysis of phosphorylated GSK3 forms (*Right*). In *B* and *C*, quantifications are displayed as mean ± SEM ($n = 3$ separate experiments), and data are statistically analyzed by one-way ANOVA (*B–D*) or by an unpaired Student's *t* test (*E*). ***$P < 0.001$; **$P < 0.01$; *$P < 0.05$, with respect Aqp8bb-Flag-WT or as indicated in brackets.

controlling Aqp8bb trafficking is absent in zebrafish spermatozoa. As observed for seabream sperm, high levels of intracellular ROS induced by PKC inhibition also reduced the percentage of motility and progressivity and the VCL of zebrafish spermatozoa (Fig. 7*C*). However, in this case Mito-TEMPO treatment only partially recovered the kinematic properties (Fig. 7*D*), suggesting that PKC plays an additional role for sperm motility and velocity maintenance in zebrafish that is unrelated to the mitochondrial peroxiporin transport mechanism.

Comparison of the deduced amino acid sequences of the Aqp8bb N terminus from seabream, salmon, and zebrafish revealed a Ser residue in position 14 or 16 in all three species, whereas the JNK Thr^{24} phosphorylation site from seabream Aqp8bb was missing in the two FW spawning teleosts. In silico analysis revealed that Ser^{14} from salmon Aqp8bb is a putative phosphorylation site for GSK3, as is Ser^{16} from seabream Aqp8bb, including a potential priming site at Ser^{18}, whereas Ser^{16} in zebrafish Aqp8bb is a presumed residue for PKC phosphorylation (Fig. 7*E*). To confirm that these target sites in salmon and zebrafish Aqp8bb are functional, in vitro phosphorylation assays were performed in HEK293 cells as described above. In this case, we tested rGSK3β and recombinant *X. laevis* PKCα (rPKCα) on Aqp8bb-Flag-WT and mutant channels, in which Aqp8bb Ser^{14} (salmon) or Ser^{16} (zebrafish) were replaced by Ala. Immunoblot results showed that salmon Aqp8bb-Flag-WT was equally phosphorylated by rPKCα and rGSK3β at Ser residues, whereas rGSK3β was no longer able to phosphorylate Ser residues

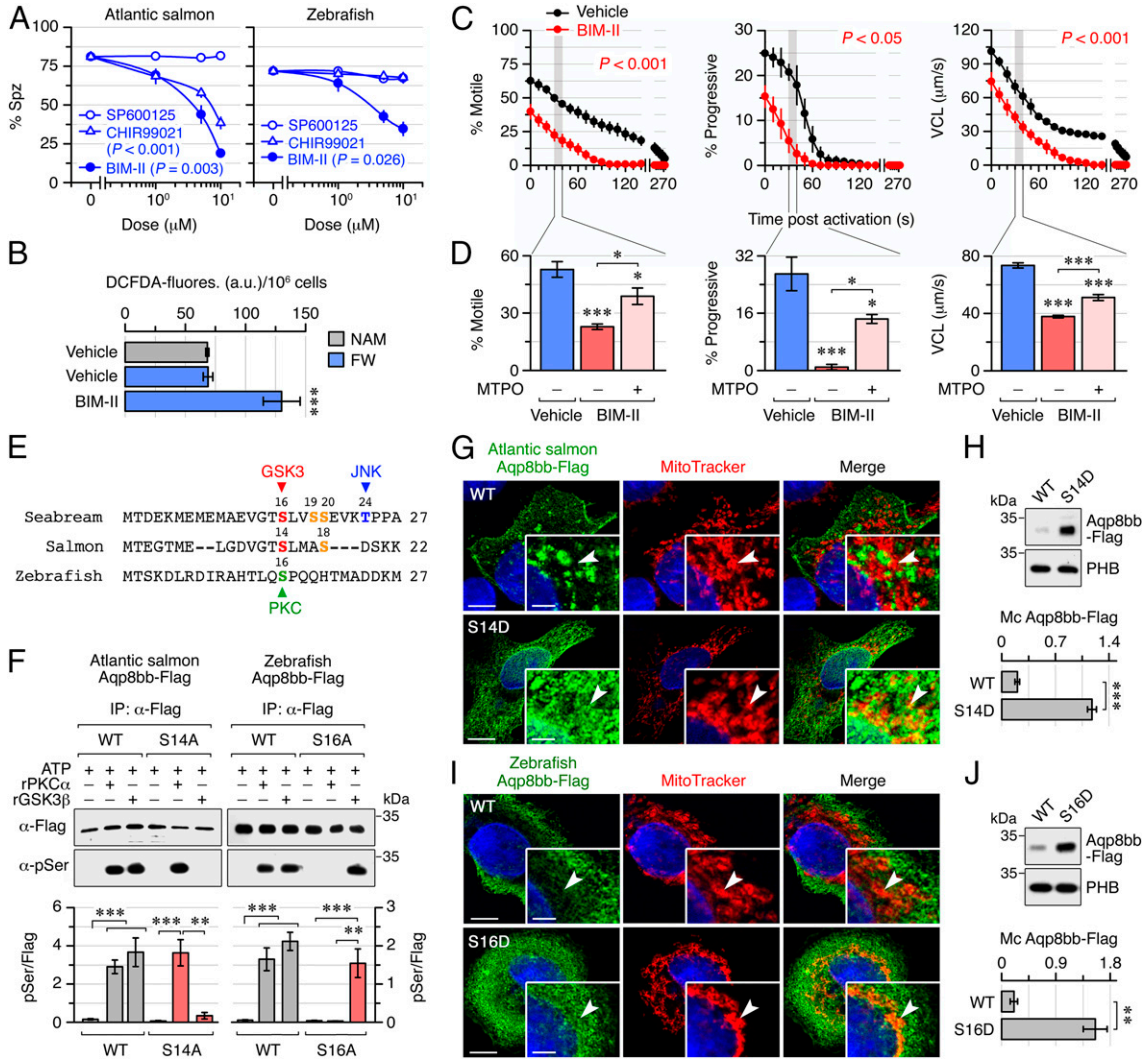

Fig. 7. Aqp8bb mitochondrial transport in FW spermatozoa is controlled by monophosphorylation of the N terminus of the channel by PKC or GSK3. (*A*) Percentage of salmon and zebrafish spermatozoa (mean ± SEM; $n = 4$ fish for salmon, and $n = 3$ pools of 5 fish for zebrafish) showing Aqp8bb mitochondrial localization after treatment with vehicle (DMSO), or JNK (SP600125), PKC (BIM-II), or GSK3 (CHIR99021) inhibitors. (*B*) ROS levels (mean ± SEM; $n = 6$ fish) in immotile and activated zebrafish spermatozoa treated with vehicle or BIM-II. (*C*) Motility, progressivity, and VCL of zebrafish activated spermatozoa (mean ± SEM, $n = 7$ fish) treated with vehicle or BIM-II. *P* values are calculated from the Mann–Whitney *U* test (during the first 60 s only for motility and progressivity). (*D*) Effect of MTPO (50 μM) on BIM-II inhibition of zebrafish sperm kinetics (mean ± SEM, $n = 5$ fish) at 30 to 40 s postactivation (gray bar in *C*). Data in *B* and *D* are statistically analyzed by one-way ANOVA (***$P < 0.001$; *$P < 0.05$, with respect to nontreated sperm). (*E*) Amino acid sequence alignment of seabream, salmon, and zebrafish Aqp8bb N terminus indicating the GSK3, PKC, and JNK phosphorylation sites. (*F*) Immunoblot of Ser phosphorylation in salmon and zebrafish Aqp8bb-Flag-WT and -S14A and -S16A mutants, respectively, after phosphorylation in vitro by rPKCα (0.08 μM) and rGSK3β (0.17 μM). (*Lower*) Quantitation of phosphorylated channel normalized to total immunoprecipitated protein. (*G* and *I*) Aqp8bb-Flag and MTR double staining of HepG2 cells expressing salmon (*G*) or zebrafish (*I*) Aqp8bb-Flag-WT and phosphomimetic mutants. Arrowheads indicate colocalized signals in the mitochondria. (Scale bars, 10 μm; *Insets*, 5 μm.) (*H* and *J*) Immunoblots of Aqp8bb-Flag-WT and mutants in mitochondrial extracts from cells shown in *G* and *I*. Data in *F*, *H*, and *J* are the mean ± SEM of three separate experiments, and are statistically analyzed by one-way ANOVA (*F*) or an unpaired Student's *t* test (*H* and *J*). ***$P < 0.001$; **$P < 0.01$, as indicated in brackets.

in the Aqp8bb-Flag-S14A mutant, and only Ser phosphorylation by rPKCα was detected (Fig. 7*F*). Similarly, zebrafish Aqp8bb-Flag-WT was Ser-phosphorylated by rPKCα and rGSK3β, but the Aqp8b-Flag-S16A mutant could only be phosphorylated by rGSK3β (Fig. 7*F*). These data indicate that salmon Aqp8bb Ser^{14} and zebrafish Aqp8bb Ser^{16} are, respectively, the target residues of rGSK3β, and rPKCα. However, both salmon and zebrafish channels contain other residues that are phosphorylated by rPKCα and rGSK3β, respectively.

Finally, we transiently expressed salmon and zebrafish Aqp8bb-Flag-WT in HepG2 cells and determined the effect of external Ca^{2+} and/or H_2O_2 on mitochondrial channel localization. In contrast to seabream, Aqp8bb immunostaining of MTR-loaded cells, as well as immunoblotting of mitochondrial extracts, showed that only Ca^{2+} was able to traffic both salmon and zebrafish Aqp8bb-Flag-WT to the mitochondria (*SI Appendix*, Fig. S10 *A* and *B*). Since Ser^{14} and Ser^{16} from salmon and zebrafish Aqp8bb are, respectively, the target sites of Ca^{2+}-activated GSK3 and PKC, we investigated whether phosphomimetic mutations at these sites could induce mitochondrial targeting of the channels. For salmon Aqp8bb, we also tested Ser^{20} in case this residue could play a role as a priming site for GSK3 phosphorylation. All constructs were expressed at similar levels in HepG2 cells (*SI Appendix*, Fig. S10 *C* and *D*), but immunostaining and immunoblotting data indicated that only the salmon Aqp8bb-Flag-S14D and zebrafish Aqp8bb-Flag-S16D mutants were constitutively targeted to the

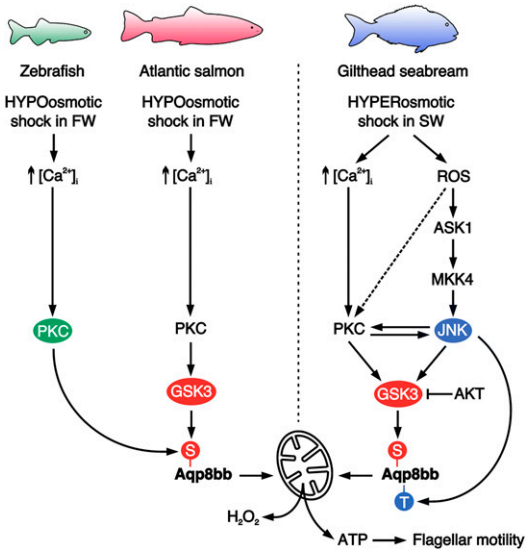

Fig. 8. A model for the evolution of the intracellular multiplier peroxiporin signal transduction pathway powering piscine spermatozoa. In spermatozoa from more primitive FW teleost lineages, such as in zebrafish and salmonids, a rise of intracellular Ca^{2+} ($[Ca^{2+}]_i$) upon activation in FW triggers the PKC-GSK3 signaling pathway, leading to the direct PKC (zebrafish) or GSK3 (Atlantic salmon) phosphorylation of N-terminal Aqp8bb residues, promoting rapid channel trafficking to the mitochondria. In modern marine teleosts such as the seabream, which release the sperm into SW, a cross-talk between $[Ca^{2+}]_i$-activated PKC and ROS-activated JNK and PKC signaling pathways converge to activate GSK3 with an additional JNK-mediated multiplier regulation of Aqp8bb mitochondrial trafficking to cope with a higher osmotic stress.

mitochondria (Fig. 7 *G–J* and *SI Appendix*, Fig. S10*C*). Taken together, these data suggest that Ca^{2+}-activated PKC or the PKC/GSK3 cascade are the effective pathways phosphorylating Ser^{16} or Ser^{14} in the N terminus of zebrafish and salmon Aqp8bb, respectively, which traffic the peroxiporin to the mitochondria.

Discussion

The present work reveals insight into the evolution of molecular mechanisms regulating spermatozoan kinematic properties in an infraclass of vertebrates that display intense levels of sperm competition. The data show that the rapid mitochondrial trafficking of an Aqp8bb peroxiporin, first discovered in a marine teleost (26), is consistently regulated through N-terminal phosphorylation in FW and SW teleosts. Such channel regulation thus represents a conserved mechanism of mitochondrial ROS detoxification for the maintenance of ATP production and improved spermatozoon performance.

The model arising from the data (Fig. 8) suggests that the signal transduction pathways regulating Aqp8bb trafficking in teleost spermatozoa evolved increasing levels of sophistication and cross-talk between the pathways through the inclusion of alternative kinase cascade modules. Thus, in older lineages of FW teleost in which spermatozoon motility is activated through hypoosmotic shock, a more direct Ca^{2+}-PKC–mediated pathway phosphorylating the Aqp8bb N terminus suffices (Fig. 8). However, in the protacanthopterygian FW salmonids, in which the importance of sperm velocity under sperm competition is well known (50), a PKC-regulated GSK3 cascade is added and the channel is only phosphorylated by GSK3 to induce its trafficking (Fig. 8). The addition of the extra GSK3 regulatory layer may act as a multiplier if the expression levels of this kinase significantly exceed those of PKC, a facet that could explain the higher sperm velocities of sedentary parasitic males compared to anadromous "bourgeois" males (51). In contrast to the FW species, we find that marine spermatozoa have recruited an addtitional ROS-triggered JNK pathway to cope with the elevated hypertonic stress (Fig. 8). In this case, JNK directly activates GSK3, but also cross-talks with Ca^{2+}- and ROS-activated PKC to trigger Aqp8bb N-terminal phosphorylation by GSK3, thus creating a multiplier pathway for the regulation of the peroxiporin trafficking. In addition, JNK bypasses the GSK3 pathway to directly phosphorylate the channel in a different N-terminal residue, further enhancing the peroxiporin trafficking.

The conserved action of PKC in each of the pathways regulating Aqp8bb trafficking in FW and SW spermatozoa reveals how the multiplier mechanism evolved. In SW-activated spermatozoa, both Ca^{2+} and ROS induce PKC activity, with ROS also inducing JNK activity through the ASK1-MKK4 cascade to further enhance PKC catalysis which, together with the direct activation of GSK3 by JNK, multiplies the action of GSK3 to phosphorylate Aqp8bb (Fig. 8). The importance of this stress-induced multiplier pathway is clearly evident on the spermatozoon kinematic properties, where JNK inhibition more rapidly suppresses the degree of motility, progressivity and velocity of spermatozoa compared to GSK3 inhibition. Consequently, it seems likely that positive selection of the JNK pathway with efficient catalytic kinetics would be advantageous in the sperm competition of SW species, while those of the PKC and GSK3 pathways would be favorable for FW species.

Interestingly, with the exception of the cross-talk between JNK and PKC to activate GSK3, we were able to replicate the signaling pathways regulating mitochondrial Aqp8bb trafficking in piscine spermatozoa in human cells. This finding suggests that these signal-transduction pathways are ancient and were likely present in the last common ancestor of mammals and fishes (>435 million y ago) (52). However, although ROS transport is involved in normal human spermatozoa functioning, and AQP8 has been observed in the midpiece and likely in the mitochondria (53, 54), it is not yet clear whether AQP8 functions as a mitochondrial peroxiporin in mammalian sperm. If indeed AQP8 is an orthologous mitochondrial peroxiporin contributing to the kinematic properties of vertebrate spermatozoa, it will be revealing to identify whether the same JNK and GSK3 pathways are involved in AQP8 trafficking mechanisms.

In mammals, the Ser/Thr kinase GSK3 is encoded by two paralogous genes (*GSK3α* and *GSK3β*), the activities of which are regulated by posttranslational Ser^{21}/Ser^{9} and Tyr^{279}/Tyr^{216} phosphorylation (37). It is now well recognized that the GSK3α enzyme plays an important role in the acquisition of sperm motility and acrosomal reaction in mammals (55–57). The inhibitory $GSK3\alpha^{S21}$ phoshorylation is high during the epididymal sperm maturation stage, but subsequently decreases to activate the kinase activity during the hyperactivation phase in the female oviduct (58–61). This latter mammalian hyperactivation mechanism is reminiscent of the activation of motility in marine fish spermatozoa (31), which is also associated with the dephosphorylation of $GSK3\alpha^{S21}$ as demonstrated here in the seabream. In teleosts, however, the role of GSK3 on spermatozoon function has remained largely unknown, although a recent study in zebrafish has shown that the knockout of miR-34a, which normally down-regulates GSK3, enhances sperm motility and the fertilization rates (62). Since we show that GSK3 is not involved in the peroxiporin trafficking mechanism in zebrafish spermatozoa, it seems likely that this kinase controls other elements of the motility. Indeed, the inability of the antioxidant mito-TEMPO to rescue seabream spermatozoa motility, when inhibited by the GSK3 blocker CHIR99021, supports the notion that GSK3 plays additional motility activation roles unrelated to Aqp8bb mitochondrial detoxification.

In contrast to GSK3, the role of the stress-activated JNK cascade for spermatozoon motility in vertebrates is less well known. This pathway is involved in both proapoptotic and antiapoptotic

mechanisms in response to various stimuli, such as osmotic and oxidative stress (63). The data available for mammalian spermatozoa suggest a role for JNK in cell survival under osmotic stress (64), as well as during progesterone-induced hyperactivation (65). Such a role of JNK during osmotic stress is consistent with the results of the present study showing the involvement of the JNK signaling pathway controlling Aqp8bb-mediated mitochondrial detoxification in marine spermatozoa. Interestingly, in the nonflagelated spermatozoa of the nematode *Caenorhabditis elegans*, both Ca^{2+} and the MAPK cascade, which functions downstream of, or parallel with, the Ca^{2+} signaling, are necessary for sperm activation (66). This resembles the molecular scenario controlling Aqp8bb trafficking in seabream spermatozoa. In addition, pharmacological activation of JNK/p38 MAPK is sufficient to trigger sperm motility acquisition in *C. elegans* (66), while the same treatment of immotile seabream sperm bypasses the requirement of the Ca^{2+} signal for the induction of mitochondrial Aqp8bb transport. Therefore, although nematode and fish spermatozoa are morphologically distinct, and their motility is regulated by different molecular machineries, both types of spermatozoa appear to utilize conserved signaling pathways for different purposes, to modulate sperm maturation in the case of the nematode, or to insert a peroxiporin in the mitochondrion of the seabream spermatozoon as an antiapoptotic mechanism.

Our pharmacological studies in seabream sperm and HepG2 cells suggest a complex cascade of kinase phosphorylation events, where PKC- and JNK-mediate GSK3 activation by GSK3α/$\beta^{Y279/216}$ phosphorylation, and PKC activates JNK and vice versa. However, both PKC and JNK are Ser/Thr kinases, and in ejaculated mammalian spermatozoa PKC inhibits, rather than activates, GSK3 activity by GSK3α^{S21} inhibitory phosphorylation (67–69). In contrast, in colon cancer cells the atypical PKCζ isoform can rapidly and transiently activate GSK3β activity through Ser^{147} phosphorylation, which is also required to maintain the constitutive basal activity of GSK3β (69). Although a PKCζ ortholog is expressed in fish sperm (70), the role of this specific kinase regulating GSK3 and Aqp8bb mitochondrial transport requires further investigation. The PKC-mediated GSK3α$\beta^{Y279/216}$ phosphorylation occurring in seabream sperm could also be an indirect mechanism, as it seems to occur during the activation of GSK3 by JNK, or the activation of JNK by PKC. The latter would resemble the Toll-like receptor 4 transient receptor potential channel 1-PKCα signaling pathway that is triggered as defense and proinflammatory response to bacterial infection (71), in which PKC may phosphorylate Ser^{129} in JNK augmenting its phosphorylation by MKK4 (72). The JNK-mediated activation of GSK3 has been reported to take place in a hepatocyte cell line through the MAP3K mixed-lineage kinase 3 in a positive feedback mechanism (73). A similar indirect mechanism mediating the activation of GSK3 by JNK might occur through stimulation of the proline-rich tyrosine kinase 2, which is a Ca^{2+}-activated tyrosine kinase in capacitated human sperm (74), or through the Src-related tyrosine kinase Fyn (75).

The present study provides evidence suggesting that piscine Aqp8bb is a physiological substrate of PKC, GSK3, and JNK, which regulate channel trafficking. This is supported by the demonstration that these kinases can phosphorylate the different teleost Aqp8bb orthologs in vitro, and that mutations of the respective target sites trigger or abolish mitochondrial channel transport. In the seabream model, it is also supported by the observation that inhibition of GSK3 and JNK activity through the expression of dominant-negative forms of the kinases in HepG2 cells specifically reduces the phosphorylation of the target sites in the channel and impairs mitochondrial trafficking. The phosphorylation of Aqp8bb by JNK at Thr^{24} could play a role as a priming mechanism for subsquent GSK3 phosphorylation since our in vitro data show that mimicking a constitutive phosphorylated state of this site can enhance GSK3 phosphorylation of Ser^{16} in the channel. This would agree with the observation that under cell stress JNK can phosphorylate antiapoptotic proteins priming them for subsequent phosphorylation by GSK3 (45). However, we found that mutation of Thr^{24} into Ala in seabream Aqp8bb to prevent its phosphorylation by JNK does not reduce GSK3-mediated Ser phosphorylation of the channel in HepG2 cells during Ca^{2+} and H_2O_2 stimulation. This therefore argues against a role of JNK as a priming kinase for GSK3. Rather, our data indicate that GSK3 and JNK phosphorylation of Aqp8bb are both required for maximum accumulation of the channel in the mitochondria.

In summary, this work presents a mechanism of spermatozoon motility regulation in animals. The data show that a conserved process of mitochondrial ROS detoxification evolved in piscine spermatozoa to enhance their kinematic properties. The detoxification process occurs through the rapid trafficking of an Aqp8bb peroxiporin to the inner mitochodrial membrane to facilitate H_2O_2 efflux and the continued production of ATP necessary for flagellar contractions. The signal transduction cascades controlling the trafficking mechanism are rapidly activated in ejaculated sperm through hydration in FW teleosts and dehydration in SW teleosts, leading to phosphorylation of Ser/Thr residues in the Aqp8bb N terminus. The data further reveal the evolution of an increasingly sophisticated hierarchy of kinases activating the trafficking mechanism with more direct Ca^{2+}-PKC or Ca^{2+}-PKC-GSK3 induction pathways in ancient lineages of FW teleosts to a cross-talk between the Ca^{2+}-PKC-GSK3 signaling mechanism and a ROS-activated JNK multiplier pathway in modern lineages of marine teleosts. These findings uncover gene networks involved in postactivated spermatozoon swimming performance and thus provide insight into the molecular controls that may form selective traits for postcopulatory sexual selection.

Materials and Methods

Detailed information on the methods employed are provided in *SI Appendix, Supplementary Materials and Methods*.

Procedures relating to the care and use of animals and sample collection were approved by the Ethics Committee of the Institute of Agrifood Research and Technology, following the European Union Council Guidelines (86/609/EU), or in accordance with the regulations approved by the governmental Norwegian Animal Research Authority (http://www.fdu.no/fdu/).

Data Availability. All study data are included in the article and *SI Appendix*.

ACKNOWLEDGMENTS. We thank Prof. S. S. Madsen for providing Atlantic salmon Aqp8aa, -8ab, and -8bb specific antibodies. This work was supported by Spanish Ministry of Economy, Industry and Competitiveness (MINECO) Grant AGL2016-76802-R (to J.C.) and Norwegian Research Council Grants 254872/E40 and 294768/E40 (to R.N.F.). F.C. and A.F. were supported, respectively, by a "Ramon y Cajal" contract (RYC-2015-17103) and a predoctoral grant (BES-2014-068745) from Spanish MINECO.

1. M. J. Gage, P. Stockley, G. A. Parker, Effects of alternative male mating strategies on characteristics of sperm production in the Atlantic salmon (*Salmo salar*): Theoretical and empirical investigations. *Philos. Trans. R. Soc. Lond. B Biol. Sci.* **350**, 391–399 (1995).
2. D. P. Froman, A. J. Feltmann, M. L. Rhoads, J. D. Kirby, Sperm mobility: A primary determinant of fertility in the domestic fowl (*Gallus domesticus*). *Biol. Reprod.* **61**, 400–405 (1999).
3. E. Kupriyanova, J. N. Havenhand, Variation in sperm swimming behaviour and its effect on fertilization success in the serpulid polychaete *Galeolaria caespitosa*. *Invertebr. Reprod. Dev.* **41**, 21–26 (2002).
4. T. Pizzari, G. A. Parker, "Sperm competition and sperm phenotype" in *Sperm Biology: An Evolutionary Perspective*, T. R. Birkhead, D. J. Hosken, S. Pitnick, Eds. (Academic Press, 2009), pp. 207–245.
5. E. Del Olmo *et al.*, Fertility of cryopreserved ovine semen is determined by sperm velocity. *Anim. Reprod. Sci.* **138**, 102–109 (2013).
6. R. K. Browne *et al.*, Sperm motility of externally fertilizing fish and amphibians. *Theriogenology* **83**, 1–13 (2015).
7. A. M. Cancel, D. Lobdell, P. Mendola, S. D. Perreault, Objective evaluation of hyperactivated motility in rat spermatozoa using computer-assisted sperm analysis. *Hum. Reprod.* **15**, 1322–1328 (2000).

8. D. R. Levitan, Sperm velocity and longevity trade off each other and influence fertilization in the sea urchin Lytechinus variegatus. *Proc. Biol. Sci.* **267**, 531–534 (2000).
9. T. R. Birkhead, F. M. Hunter, Mechanisms of sperm competition. *Trends Ecol. Evol.* **5**, 48–52 (1990).
10. M. J. Gage *et al*., Spermatozoal traits and sperm competition in Atlantic salmon: Relative sperm velocity is the primary determinant of fertilization success. *Curr. Biol.* **14**, 44–47 (2004).
11. S. Liljedal, G. Rudolfsen, I. Foldstad, Factors predicting male fertilization success in an external fertilizer. *Behav. Ecol. Sociobiol.* **62**, 1805–1811 (2008).
12. J. L. Fitzpatrick *et al*., Female promiscuity promotes the evolution of faster sperm in cichlid fishes. *Proc. Natl. Acad. Sci. U.S.A.* **106**, 1128–1132 (2009).
13. C. Gasparini, L. W. Simmons, M. Beveridge, J. P. Evans, Sperm swimming velocity predicts competitive fertilization success in the green swordtail *Xiphophorus helleri*. *PLoS One* **5**, e12146 (2010).
14. C. Boschetto, C. Gasparini, A. Pilastro, Sperm number and velocity affect sperm competition success in the guppy (*Poecilia reticulata*). *Behav. Ecol. Sociobiol.* **65**, 813–821 (2011).
15. M. Tourmente, M. Gomendio, E. R. Roldan, Sperm competition and the evolution of sperm design in mammals. *BMC Evol. Biol.* **11**, 12 (2011).
16. G. A. Parker, Sperm competition and its evolutionary consequences in the insects. *Biol. Rev. Camb. Philos. Soc.* **45**, 525–567 (1970).
17. G. A. Parker, T. Pizzari, Sperm competition and ejaculate economics. *Biol. Rev. Camb. Philos. Soc.* **85**, 897–934 (2010).
18. P. Stockley, M. J. G. Gage, G. A. Parker, A. P. Møller, Sperm competition in fishes: The evolution of testis size and ejaculate characteristics. *Am. Nat.* **149**, 933–954 (1997).
19. A. Civetta, J. M. Ranz, Genetic factors influencing sperm competition. *Front. Genet.* **10**, 820 (2019).
20. R. C. Firman, L. W. Simmons, Sperm midpiece length predicts sperm swimming velocity in house mice. *Biol. Lett.* **6**, 513–516 (2010).
21. T. V. Vladić, B. A. Afzelius, G. E. Bronnikov, Sperm quality as reflected through morphology in salmon alternative life histories. *Biol. Reprod.* **66**, 98–105 (2002).
22. S. Lüpold, S. Calhim, S. Immler, T. R. Birkhead, Sperm morphology and sperm velocity in passerine birds. *Proc. Biol. Sci.* **276**, 1175–1181 (2009).
23. E. de Lamirande, C. Gagnon, Reactive oxygen species and human spermatozoa. I. Effects on the motility of intact spermatozoa and on sperm axonemes. *J. Androl.* **13**, 368–378 (1992).
24. E. de Lamirande, C. Gagnon, Reactive oxygen species and human spermatozoa. II. Depletion of adenosine triphosphate plays an important role in the inhibition of sperm motility. *J. Androl.* **13**, 379–386 (1992).
25. J. S. Armstrong *et al*., Characterization of reactive oxygen species induced effects on human spermatozoa movement and energy metabolism. *Free Radic. Biol. Med.* **26**, 869–880 (1999).
26. F. Chauvigné, M. Boj, R. N. Finn, J. Cerdà, Mitochondrial aquaporin-8-mediated hydrogen peroxide transport is essential for teleost spermatozoon motility. *Sci. Rep.* **5**, 7789 (2015).
27. S. Sadeghi *et al*., Effect of different oxidative stress degrees generated by hydrogen peroxide on motility and DNA fragmentation of zebrafish (*Danio rerio*) spermatozoa. *Reprod. Domest. Anim.* **53**, 1498–1505 (2018).
28. L. Burnaugh, B. A. Ball, K. Sabeur, A. D. Thomas, S. A. Meyers, Osmotic stress stimulates generation of superoxide anion by spermatozoa in horses. *Anim. Reprod. Sci.* **117**, 249–260 (2010).
29. R. N. Finn, F. Chauvigné, J. B. Hlidberg, C. P. Cutler, J. Cerdà, The lineage-specific evolution of aquaporin gene clusters facilitated tetrapod terrestrial adaptation. *PLoS One* **9**, e113686 (2014).
30. E. Koren, J. Lukac, Mechanism of liquefaction of the human ejaculate. I. Changes of the ejaculate proteins. *J. Reprod. Fertil.* **56**, 493–499 (1979).
31. J. Cosson *et al*., Marine fish spermatozoa: Racing ephemeral swimmers. *Reproduction* **136**, 277–294 (2008).
32. J. Cosson, "Fish sperm physiology: Structure, factors regulating motility, and motility evaluation" in *Biological Research in Aquatic Science*, Y. Bozkurt, Ed. (IntechOpen, 2019), 10.5772/intechopen.85139.
33. G. N. Cherr *et al*., Two egg-derived molecules in sperm motility initiation and fertilization in the Pacific herring (*Clupea pallasi*). *Int. J. Dev. Biol.* **52**, 743–752 (2008).
34. R. J. Davis, Signal transduction by the JNK group of MAP kinases. *Cell* **103**, 239–252 (2000).
35. M. Yan *et al*., Activation of stress-activated protein kinase by MEKK1 phosphorylation of its activator SEK1. *Nature* **372**, 798–800 (1994).
36. E. H. Goldman, L. Chen, H. Fu, Activation of apoptosis signal-regulating kinase 1 by reactive oxygen species through dephosphorylation at serine 967 and 14-3-3 dissociation. *J. Biol. Chem.* **279**, 10442–10449 (2004).
37. E. Beurel, S. F. Grieco, R. S. Jope, Glycogen synthase kinase-3 (GSK3): Regulation, actions, and diseases. *Pharmacol. Ther.* **148**, 114–131 (2015).
38. D. R. Alessi, A. Cuenda, P. Cohen, D. T. Dudley, A. R. Saltiel, PD 098059 is a specific inhibitor of the activation of mitogen-activated protein kinase kinase in vitro and in vivo. *J. Biol. Chem.* **270**, 27489–27494 (1995).
39. A. P. Kozikowski, H. Sun, J. Brognard, P. A. Dennis, Novel PI analogues selectively block activation of the pro-survival serine/threonine kinase Akt. *J. Am. Chem. Soc.* **125**, 1144–1145 (2003).
40. S. F. Moore *et al*., Dual regulation of glycogen synthase kinase 3 (GSK3)α/β by protein kinase C (PKC)α and Akt promotes thrombin-mediated integrin αIIbβ3 activation and granule secretion in platelets. *J. Biol. Chem.* **288**, 3918–3928 (2013).
41. M. Boj, F. Chauvigné, J. Cerdà, Coordinated action of aquaporins regulates sperm motility in a marine teleost. *Biol. Reprod.* **93**, 40 (2015).
42. A. Matsuzawa, H. Ichijo, Redox control of cell fate by MAP kinase: Physiological roles of ASK1-MAP kinase pathway in stress signaling. *Biochim. Biophys. Acta* **1780**, 1325–1336 (2008).
43. M. Hagedorn, M. McCarthy, V. L. Carter, S. A. Meyers, Oxidative stress in zebrafish (*Danio rerio*) sperm. *PLoS One* **7**, e39397 (2012).
44. Y. Li, M. A. Trush, Diphenyleneiodonium, an NAD(P)H oxidase inhibitor, also potently inhibits mitochondrial reactive oxygen species production. *Biochem. Biophys. Res. Commun.* **253**, 295–299 (1998).
45. C. Sutherland, What are the bona fide GSK3 Substrates? *Int. J. Alzheimers Dis.* **2011**, 505607 (2011).
46. X. Ren, X. Chen, Z. Wang, D. Wang, Is transcription in sperm stationary or dynamic? *J. Reprod. Dev.* **63**, 439–443 (2017).
47. M. J. Marchissio, D. E. Francés, C. E. Carnovale, R. A. Marinelli, Mitochondrial aquaporin-8 knockdown in human hepatoma HepG2 cells causes ROS-induced mitochondrial depolarization and loss of viability. *Toxicol. Appl. Pharmacol.* **264**, 246–254 (2012).
48. V. F. Taelman *et al*., Wnt signaling requires sequestration of glycogen synthase kinase 3 inside multivesicular endosomes. *Cell* **143**, 1136–1148 (2010).
49. B. Dérijard *et al*., JNK1: A protein kinase stimulated by UV light and Ha-Ras that binds and phosphorylates the c-Jun activation domain. *Cell* **76**, 1025–1037 (1994).
50. J. Beirão, T. B. Egeland, C. F. Purchase, J. T. Nordeide, Fish sperm competition in hatcheries and between wild and hatchery origin fish in nature. *Theriogenology* **133**, 201–209 (2019).
51. M. Taborsky, Sperm competition in fish: 'Bourgeois' males and parasitic spawning. *Trends Ecol. Evol.* **13**, 222–227 (1998).
52. S. Kumar, G. Stecher, M. Suleski, S. B. Hedges, TimeTree: A resource for timelines, timetrees, and divergence times. *Mol. Biol. Evol.* **34**, 1812–1819 (2017).
53. U. Laforenza *et al*., Aquaporin-mediated water and hydrogen peroxide transport is involved in normal human spermatozoa functioning. *Int. J. Mol. Sci.* **18**, 66 (2016).
54. G. Pellavio *et al*., HPV infection affects human sperm functionality by inhibition of Aquaporin-8. *Cells* **9**, 1241 (2020).
55. R. Bhattacharjee *et al*., Targeted disruption of glycogen synthase kinase 3A (GSK3A) in mice affects sperm motility resulting in male infertility. *Biol. Reprod.* **92**, 65 (2015).
56. A. T. Reid *et al*., Glycogen synthase kinase 3 regulates acrosomal exocytosis in mouse spermatozoa via dynamin phosphorylation. *FASEB J.* **29**, 2872–2882 (2015).
57. S. Dey *et al*., Roles of glycogen synthase kinase 3 alpha and calcineurin in regulating the ability of sperm to fertilize eggs. *FASEB J.* **34**, 1247–1269 (2020).
58. S. Koch, S. P. Acebron, J. Herbst, G. Hatiboglu, C. Niehrs, Post-transcriptional Wnt signaling governs epididymal sperm maturation. *Cell* **163**, 1225–1236 (2015).
59. M. J. Freitas *et al*., Isoform-specific GSK3A activity is negatively correlated with human sperm motility. *Mol. Hum. Reprod.* **25**, 171–183 (2019).
60. S. Dey, C. Brothag, S. Vijayaraghavan, Signaling enzymes required for sperm maturation and fertilization in mammals. *Front. Cell Dev. Biol.* **7**, 341 (2019).
61. D. Martin-Hidalgo, R. Serrano, C. Zaragoza, L. J. Garcia-Marin, M. J. Bragado, Human sperm phosphoproteome reveals differential phosphoprotein signatures that regulate human sperm motility. *J. Proteomics* **215**, 103654 (2020).
62. W. Guo *et al*., miR-34a regulates sperm motility in zebrafish. *Int. J. Mol. Sci.* **18**, 2676 (2017).
63. J. Yue, J. M. López, Understanding MAPK signaling pathways in apoptosis. *Int. J. Mol. Sci.* **21**, 2346 (2020).
64. B. M. García *et al*., The mitochondria of stallion spermatozoa are more sensitive than the plasmalemma to osmotic-induced stress: Role of c-Jun N-terminal kinase (JNK) pathway. *J. Androl.* **33**, 105–113 (2012).
65. V. Sagare-Patil *et al*., Differential concentration and time dependent effects of progesterone on kinase activity, hyperactivation and acrosome reaction in human spermatozoa. *Int. J. Androl.* **35**, 633–644 (2012).
66. Z. Liu, B. Wang, R. He, Y. Zhao, L. Miao, Calcium signaling and the MAPK cascade are required for sperm activation in *Caenorhabditis elegans*. *Biochim. Biophys. Acta* **1843**, 299–308 (2014).
67. I. M. Aparicio *et al*., Porcine sperm motility is regulated by serine phosphorylation of the glycogen synthase kinase-3alpha. *Reproduction* **134**, 435–444 (2007).
68. M. J. Bragado, I. M. Aparicio, M. C. Gil, L. J. Garcia-Marin, Protein kinases A and C and phosphatidylinositol 3 kinase regulate glycogen synthase kinase-3A serine 21 phosphorylation in boar spermatozoa. *J. Cell. Biochem.* **109**, 65–73 (2010).
69. N. Tejeda-Muñoz, H. González-Aguilar, P. Santoyo-Ramos, M. C. Castañeda-Patlán, M. Robles-Flores, Glycogen synthase kinase 3β is positively regulated by protein kinase Cζ-mediated phosphorylation induced by Wnt agonists. *Mol. Cell. Biol.* **36**, 731–741 (2015).
70. C. F. Huang, H. C. Chen, N. N. Chuang, C. M. Kuo, The zeta protein kinase C isoform from the testis of the grey mullet *Mugil cephalus* with a specific reaction protein of M(r) 48,000 on oolemma. *Comp. Biochem. Physiol. C Pharmacol. Toxicol. Endocrinol.* **111**, 429–433 (1995).
71. X. Zhou *et al*., Transient receptor potential channel 1 deficiency impairs host defense and proinflammatory responses to bacterial infection by regulating protein kinase Cα signaling. *Mol. Cell. Biol.* **35**, 2729–2739 (2015).
72. P. López-Bergami *et al*., RACK1 mediates activation of JNK by protein kinase C [corrected]. *Mol. Cell* **19**, 309–320 (2005).
73. M. Sharma, V. Gadang, A. Jaeschke, Critical role for mixed-lineage kinase 3 in acetaminophen-induced hepatotoxicity. *Mol. Pharmacol.* **82**, 1001–1007 (2012).
74. N. G. Brukman *et al*., Tyrosine phosphorylation signaling regulates Ca^{2+} entry by affecting intracellular pH during human sperm capacitation. *J. Cell. Physiol.* **234**, 5276–5288 (2019).
75. M. Lesort, R. S. Jope, G. V. Johnson, Insulin transiently increases tau phosphorylation: Involvement of glycogen synthase kinase-3beta and Fyn tyrosine kinase. *J. Neurochem.* **72**, 576–584 (1999).

PNAS
www.pnas.org

Supplementary Information for:

A multiplier peroxiporin signal transduction pathway powers piscine spermatozoa

François Chauvigné, Alba Ferré, Carla Ducat, Tom Hansen, Montserrat Carrascal, Joaquín Abián, Roderick Nigel Finn and Joan Cerdà

Joan Cerdà
Email: joan.cerda@irta.cat

This PDF file includes:

Supplementary Text S1

The Aqp8bb spermatozoon mitochondrial transport pathway can be replicated in human HepG2 cells. We transiently transfected the HepG2 cells with seabream Aqp8bb-Flag and exposed them to external 10 mM of Ca^{2+} and/or 100 μM H_2O_2, which elicit maximum intracellular levels of the solutes (Fig. S8*A*). Immunolabelling of Aqp8bb-Flag in cells loaded with MitoTracker to stain mitochondria shows that both Ca^{2+} and H_2O_2 trigger the co-localization of Aqp8bb and MitoTracker signals, suggesting the activation of channel transport into the mitochondria (Fig. S8*B*). These observations are corroborated by Aqp8bb-Flag immunoblotting of mitochondrial extracts, which also show that when both compounds are present the accumulation of the channel in the mitochondria approximately doubles (Fig. S8*C*). This suggests that Ca^{2+} and H_2O_2 activate independent and additive signaling pathways in HepG2 cells controlling Aqp8bb trafficking as observed in seabream spermatozoa.

The stimulatory effect of Ca^{2+} on Aqp8bb mitochondrial transport in HepG2 cells is associated with the activation of GSK3 but not of JNK, whereas H_2O_2 triggers the activation of both JNK and GSK3 (Fig. S8*D*). When cells are exposed to both Ca^{2+} and H_2O_2 the activation of JNK is similar to that seen with H_2O_2 alone, while that of GSK3 is approximately the double with respect to that noted with Ca^{2+} or H_2O_2 (Fig. S8*D*). The inhibitory GSK3α^{S21} phosphorylation is equally reduced by Ca^{2+} or H_2O_2 treatment, and this seems to decrease further using both compounds together (Fig. S8*D*), suggesting that Ca^{2+} and H_2O_2 increase GSK3 activity in HepG2 cells by enhancing and decreasing Gsk3α/β$^{Y279/216}$ and GSK3α^{S21} phosphorylation, respectively.

The inhibition of PKC, JNK and GSK3 during Ca^{2+} and/or H_2O_2-triggered Aqp8bb mitochondrial transport, using BIM-II, SP600125 and CHIR99021, respectively, show that PKC and GSK3, but not JNK, are essential for Ca^{2+}-mediated partial channel transport (Fig. S8*E*), possibly through PKC activation of GSK3, since only PKC inhibition decreased GSK3α/β$^{Y279/216}$ phosphorylation (Fig. S8*F*). In contrast, JNK and GSK3, but not PKC, are involved in the stimulatory effect of H_2O_2 on Aqp8bb trafficking, through JNK activation, which increases GSK3α/β$^{Y279/216}$ phosphorylation (Fig. S8 *E* and *F*). Interestingly, Ca^{2+}+H_2O_2-triggered Aqp8bb trafficking is strongly reduced after JNK and GSK3 inhibition, but only partially blocked by the PKC inhibitor (Fig. S8*E*). However, both JNK and PKC inhibitors reduced GSK3 activation to a similar extent (Fig. S8*F*), which suggest a direct action of JNK driving Aqp8bb transport, in addition to that mediated by GSK3, as found in seabream sperm.

Together, these data indicate that the same PKC-GSK3 and JNK-GSK3 signaling cascades that control Aqp8bb mitochondrial transport in the seabream spermatozoon can be replicated in HepG2 cells (Fig. S8*G*), except that in these human cells the cross-talk between PKC and JNK does not occur.

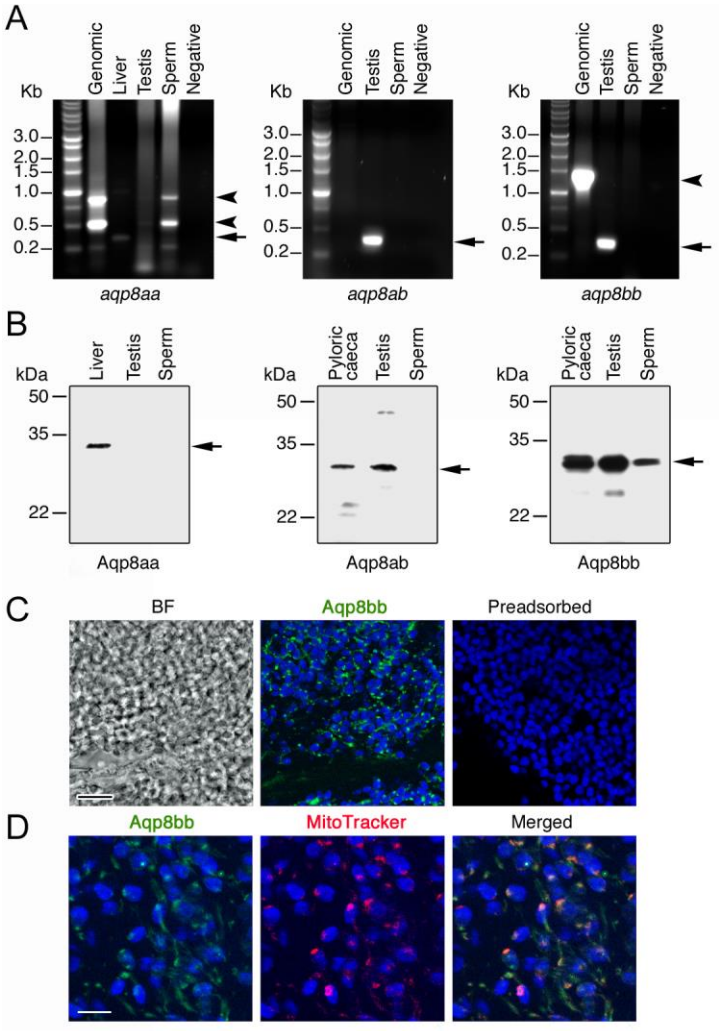

Fig. S1. The Atlantic salmon (*Salmo salar*) Aqp8bb peroxiporin, but not the Aqp8aa or -8ab paralogs, is expressed in spermatozoa. (*A*) RT-PCR analysis of *aqp8aa, -8ab* and *-8bb* expression in different tissues of adult fish. Genomic DNA is used as positive controls, whereas the absence of RT during cDNA synthesis (Negative) is the negative control. The arrows indicate transcripts, whereas the arrowheads indicate genomic products. The size (kb) of PCR products and molecular markers are indicated on the left. (*B*) Immunoblots for Aqp8aa, -8ab and -8bb in different tissues using Atlantic salmon paralog-specific antibodies (Table S4) show that only the Aqp8bb paralog is expressed in spermatozoa. Arrows indicate aquaporin monomers. Molecular mass markers (kDa) are on the left. (*C*) Representative brightfield (BF) and immunofluorescence microscopy images of Aqp8bb immunolocalization (green) in testicular spermatozoa of Atlantic salmon using the Aqp8bb-specific antibody. Control sections incubated with preabsorbed antisera are negative (right). (*D*) Double staining for Aqp8bb (green) and MTR (red) shows that the channel does not localize in the mitochondria in most of the intratesticular spermatozoa. In *C* and *D*, nuclei are stained with DAPI (blue). Scales bars, 10 µm (*C*), 5 µm (*D*).

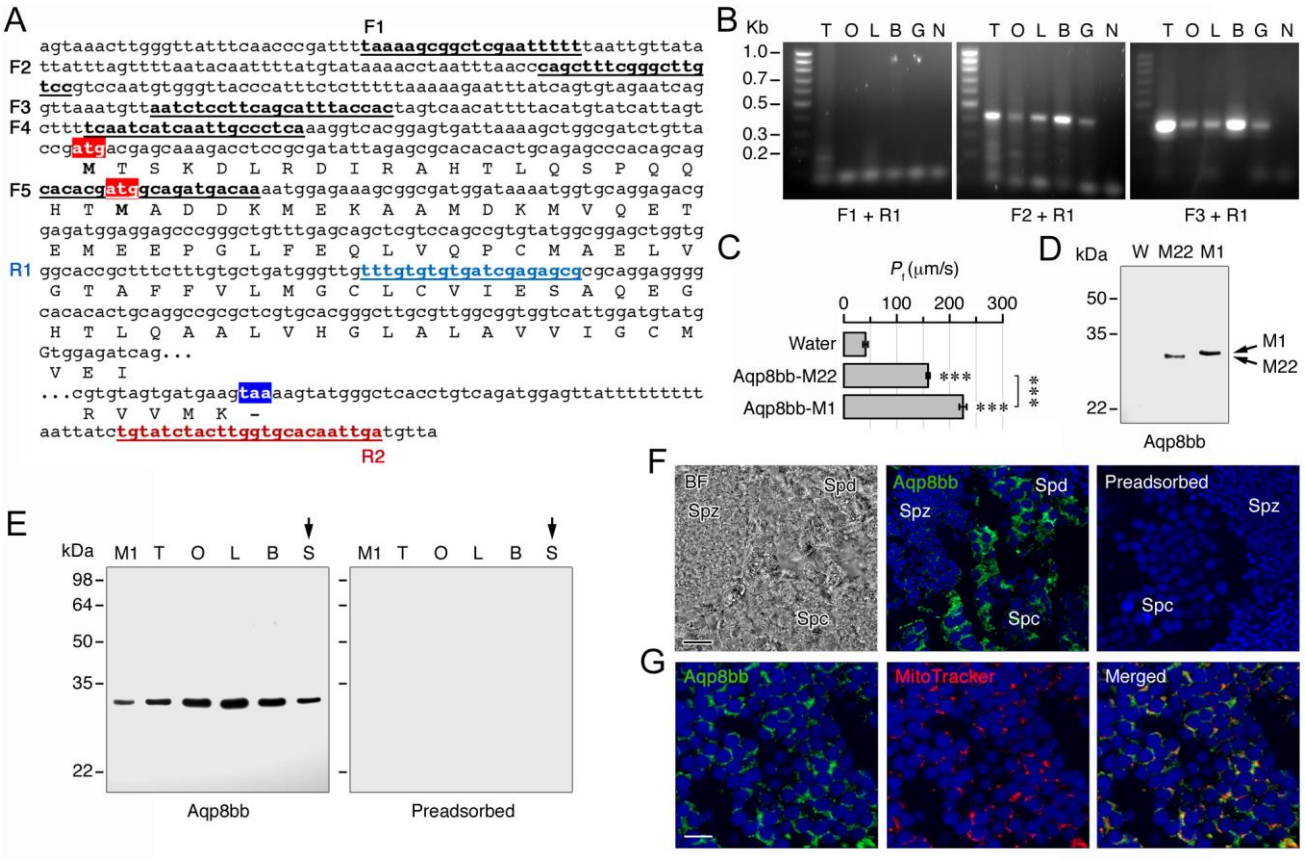

Fig. S2. Cloning and functional characterization of the complete zebrafish Aqp8bb paralog with an extended N-terminal domain. (*A*) Partial genomic sequence of exon 1 and upstream region, and of the end of exon 5 and downstream region, of the zebrafish *aqp8bb* locus (Ensembl chromosome: Zv9:3:18301156:18305325). The deduced amino acid sequence is shown below; two potential translation initiation codons (M1 and M22) are highlighted in red, whereas the stop codon is in blue. (*B*) Partial amplification of the 5' end *aqp8bb* mRNA (containing the N-terminus of the deduced protein) in different adult tissues (T, testis; O, ovary; L, liver; B, brain; G, gills) using different forward primers underlined in bold (F1, F2 and F3) and a reverser primer underlined in blue (R1), mapped in a, as indicated in each panel. The N indicates absence of RT during cDNA synthesis. The results show the amplification of a single mRNA species with F2 and F3 primers in all tissues examined, suggesting the absence of 5' end mRNA splicing. (*C*) Osmotic water permeability (P_f) of *Xenopus laevis* oocytes injected with water (control) or expressing Aqp8bb cRNAs (15 ng) bearing the translation initiation codons at M1 or M22. The corresponding full-length cDNAs are cloned using primers F4 or F5 and R2 (red color), mapped in *A*, from testis total RNA. Data are the mean ± SEM (*n* = 14-15 oocytes), and are statistically analyzed by one-way ANOVA. ***P < 0.001, with respect to water-injected oocytes or as indicated in brackets. (*D*) Immunoblot of control, Aqp8bb-M1 or -M22 oocytes using a zebrafish Aqp8bb specific antibody raised against the C-terminus (Table S1). The results in *C* and *D* indicate that both Aqp8bb-M1 and Aqp8bb-M22 are expressed at approximately the same level, while the M1 channel is more permeable than M22, suggesting that the latter cDNA sequence previously reported (GenBank accession no. NM_001114910), is lacking part of the N-terminus. (*E*) Immunoblot analysis of Aqp8bb in different adult tissues (as in *B*; S, non-activated intratesticular sperm, arrow) reveals a single reactive band with an apparent molecular mass similar to that of the Aqp8bb-M1 polypeptide (lane M1 in the blot) (left panel). A duplicated blot was run in parallel using the primary antibody preadsorbed with the antigenic peptide to test for specificity (right panel). The data suggest the absence of alternative translation initiation sites *in vivo*, and therefore, the Aqp8bb-M1 cDNA most likely encodes for the complete zebrafish Aqp8bb paralog. In *D* and *E*, molecular mass markers (kDa) are on the left. (*F*) Representative brightfield and immunofluorescence microscopy images of Aqp8bb immunolocalization (green) in the testis. Control sections incubated with preabsorbed antisera are negative (right). (*G*) Double immunostaining for Aqp8bb (green) and MTR (red) shows that the channel is expressed in the intratesticular spermatozoa but that it does not localize in the mitochondria in most of the cells. In *F* and *G*, nuclei are stained with DAPI (blue). Scale bars, 10 µm (*F*), 5 µm (*G*). Spc, spermatocytes; Spd, Spermatids; Spz, spermatozoa.

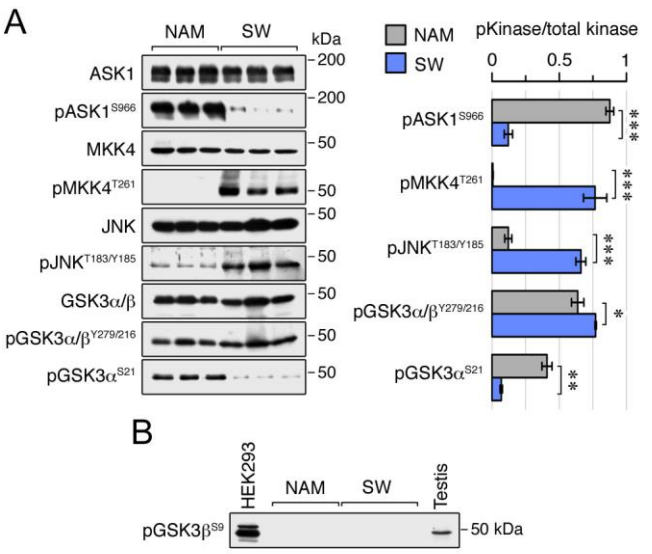

Fig. S3. Immunoblot analysis of kinase phosphorylation in seabream spermatozoa upon motility activation in SW. (*A*) Total and phosphorylated Ask1, Mkk4, Jnk and Gsk3 immunoblots in sperm from 3 males maintained in NAM or activated in SW (left panels). The right panel shows the densitometric analysis (mean ± SEM; $n = 3$ fish) of kinase phosphorylation normalized to the corresponding band from the total kinase blot. Statistical differences were determined by the unpaired Student *t* test. ***$P < 0.001$; **$P < 0.01$; *$P < 0.05$, with respect to sperm in NAM. (*B*) Immunoblotting detection of pGsk3β^{S9} in HEK293 cultured cells and seabream testis, but not in sperm either in NAM or SW ($n = 3$ fish each), suggesting that phosphorylation of Gsk3β possibly does not play a role during sperm activation in seabream spermatozoa.

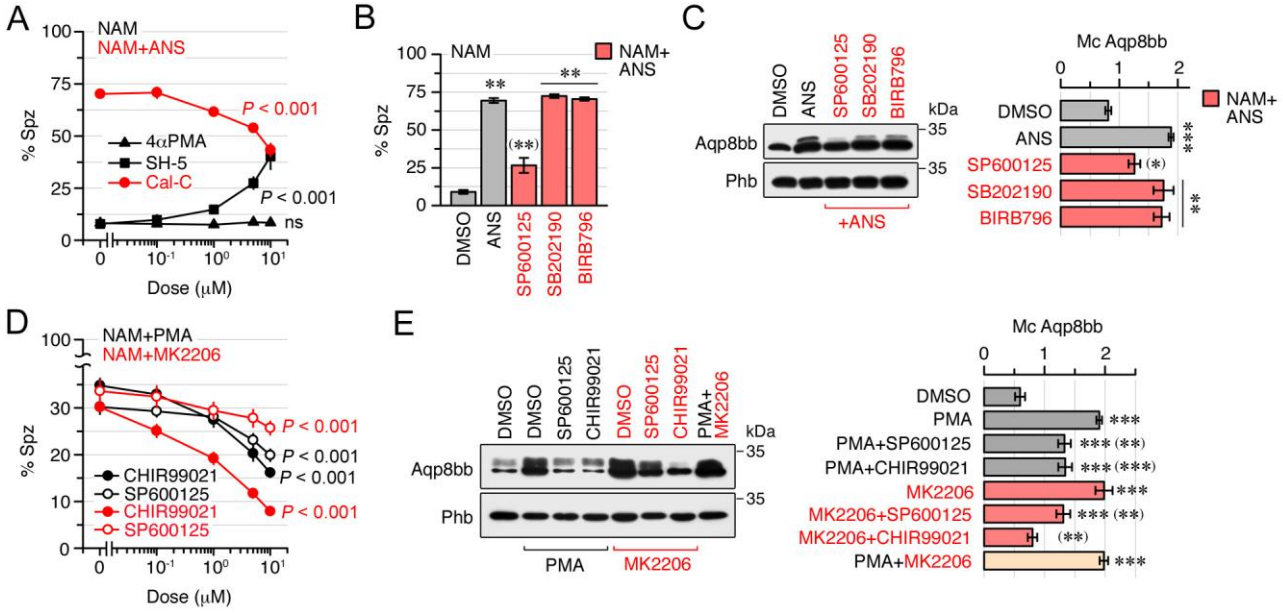

Fig. S4. Additional modulators of Aqp8bb mitochondrial trafficking in immotile seabream spermatozoa. (*A*) Dose-response activation or inhibition of Aqp8bb mitochondrial transport, determined by immunofluorescence microscopy. Sperm maintained in NAM was exposed to an inhibitor of AKT/PKB (SH-5), or to the 4-alpha-PMA (4α-PMA) negative control (black color), while ANS (10 μM)-treated sperm in NAM is incubated with a PKC inhibitor (Cal-C) (red color). (*B*, *C*) Effect of the JNK inhibitor SP600125, and two p38 MAPK inhibitors (SB202190 and BIRB796) (10 μM) on ANS-induced Aqp8bb mitochondrial trafficking in spermatozoa determined by immunofluorescence microscopy (*B*) and immunoblotting of mitochondrial extracts (*C*). The right panel in *C* is the corresponding quantitation of mitochondrial Aqp8bb normalised to Phb. (*D*, *E*) Effect of JNK and GSK3 inhibitors (SP600125 and CHIR99021, respectively) on PMA and/or MK2206-induced Aqp8bb trafficking determined as above. In all panels, data are the mean ± SEM (n = 3-5, 3, 3, 3-5, and 6 different fish, in *A*, *B*, *C*, *D* and *E*, respectively). Statistical differences are measured by one-way ANOVA (*P*-values for each compound are indicated in a and d). ***$P < 0.001$; **$P < 0.01$, with respect to non-treated spermatozoa in NAM, or with respect to sperm treated with ANS, PMA or MK2206 alone (in parenthesis).

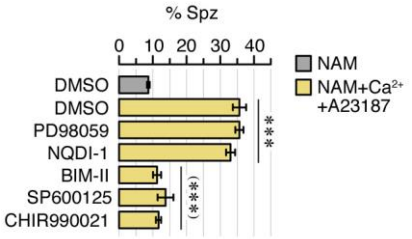

Fig. S5. Inhibition of Ca^{2+}-induced Aqp8bb trafficking in seabream spermatozoa. Effect of different kinase inhibitors (10 μM) on the percentage of immotile seabream spermatozoa showing Aqp8bb mitochondrial localization after incubation in Ca^{2+}+A23187 determined by immunofluorescence microscopy. Data (mean ± SEM; *n* = 5 fish) are statistically analyzed by one-way ANOVA. ****P* < 0.001, with respect to untreated sperm in NAM, or treated with DMSO alone in Ca^{2+}+A23187 (parenthesis).

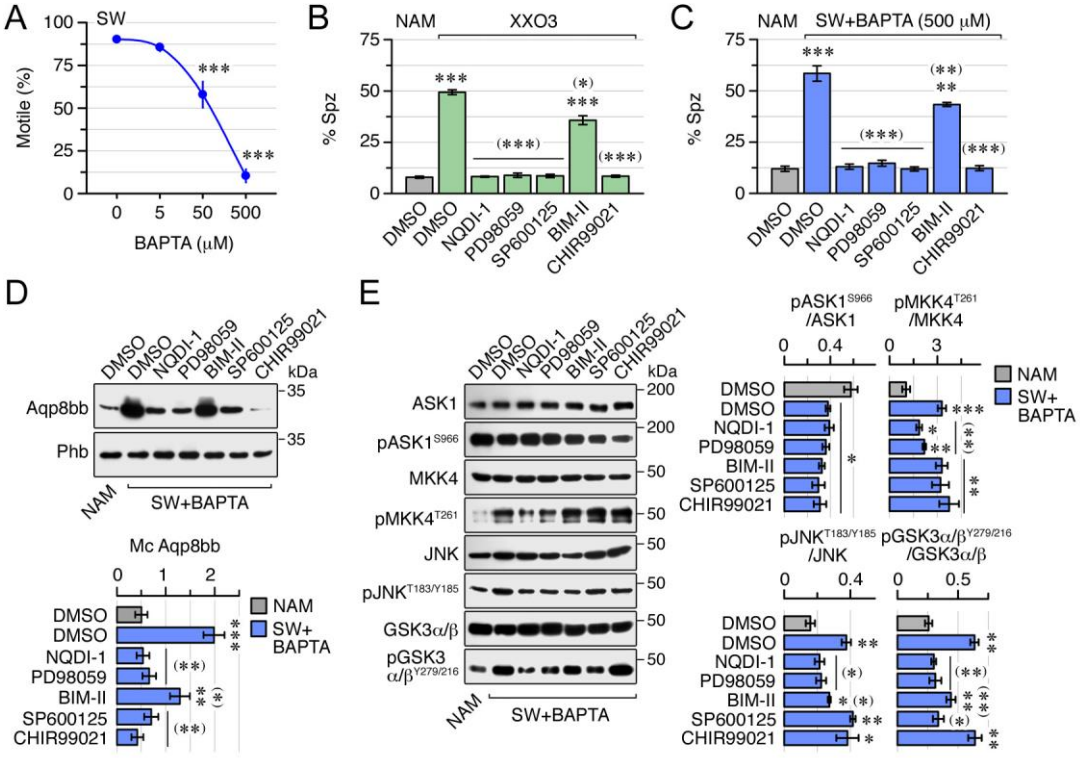

Fig. S6. (*A*) Percentage of motility of seabream sperm activated in SW containing increasing doses of BAPTA. (*B*, *C*) Percentage of spermatozoa in NAM and after treatment with XXO3 (*B*) or SW+BAPTA (*C*) showing Aqp8bb in the mitochondrion, and after treatment with kinase inhibitors (10 μM). (*D*) Representative immunoblot of Aqp8bb in the mitochondria of sperm activated in SW+BAPTA in the presence of kinase inhibitors as in *C* (upper panels), and corresponding quantitation normalised to Phb (lower panel). (*E*) Total and phosphorylated ASK1, MKK4, JNK and GSK3α/β representative immunoblots (left panels), and densitometric analysis of phosphorylated forms normalized to the corresponding non-phosphorylated bands (right panels), in spermatozoa treated as in *C* and *D*. In all panels, data are the mean ± SEM (*n* = 7 fish in *A*, *n* = 5 fish in *B* and *C*, *n* = 6 fish in *D*, and *n* = 4 in *E*), and are statistically analyzed by one-way ANOVA. ****P* < 0.001; ***P* < 0.01; **P* < 0.05, with respect to untreated sperm in NAM, or treated with DMSO alone in XXO3 or SW+BAPTA (in parenthesis).

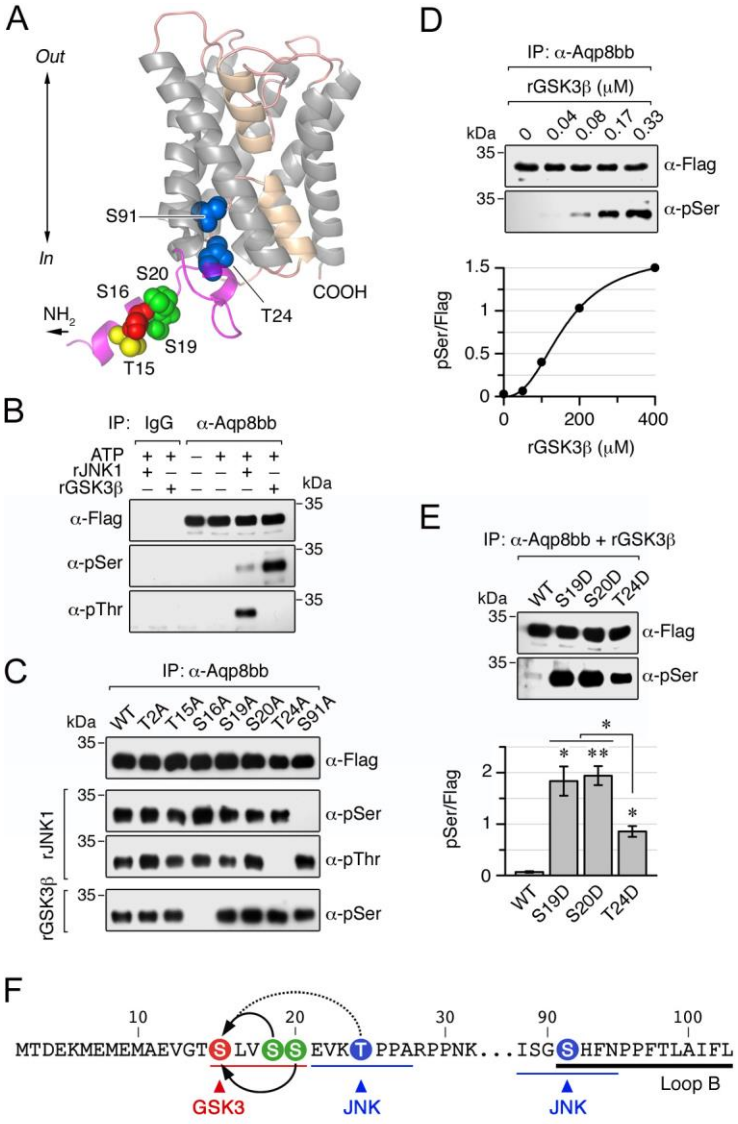

Fig. S7. Phosphorylation of seabream Aqp8bb by GSK3 and JNK *in vitro*. (*A*) Mirrored lateral view of seabream Aqp8bb, rendered by MacPymol using orthologous *Pichia pastoris* Aqy1 (3ZOJ) as the structure mask. The render shows all potential Ser and Thr phosphorylation sites (spacefill) in the N-terminus (magenta), except Thr^{2}, with Ser^{91} in the cytoplasmic loop B. The predicted phosphorylation sites by GSK3 (Ser^{16}, Ser^{19} and Ser^{20}) and proline-directed kinase (Thr^{24}), such as JNK, are indicated in red and blue color, respectively. The Ser^{91} shows low mixed score for GSK3/proline-directed kinase phosphorylation. (*B*) Immunoblot of Ser and Thr phosphorylation of immunoprecipitated Aqp8bb-Flag from transfected HEK293T cells by recombinant JNK1 (rJNK1; 0.11 μM) or GSK3β (rGSK3β; 0.17 μM), in the presence or absence of 200 μM ATP. Immunoprecipitation with rabbit immunoglobulin G (IgG) is used as control. (*C*) *In vitro* phosphorylation of wild-type Aqp8bb-Flag (WT) and single mutants determined as above. A representative blot of two independent experiments is shown. (*D*) Dose-response in Ser phosphorylation of immunoprecipitated wild-type Aqp8bb-Flag after incubation with increasing amounts of rGSK3β and 200 μM ATP. The lower panel shows the corresponding quantitation of Aqp8bb-Flag Ser phosphorylation normalised to the total immunoprecipitated protein. Data are the mean of 2 independent experiments. (*E*) Immunoblot of Ser^{16} phosphorylation in Aqp8bb-Flag-WT and Aqp8bb-S19D, -S20D and -T24D phosphomimetic mutants by rGSK3β (0.08 μM). The lower panel shows the corresponding quantitation (mean ± SEM; $n = 3$ independent experiments) of phosphorylated Aqp8bb-Flag normalised as above. Data are statistically analyzed by one-way ANOVA. $^{**}P < 0.01$; $^{*}P < 0.05$, with respect to the WT, or as indicated in brackets. (*F*) Schematic representation of the seabream Aqp8bb N-terminus and loop B showing potential priming sites (Ser^{19}, Ser^{20} and Thr^{24}) for Ser^{16} phosphorylation by rGSK3β (arrows). Consensus sequences for GSK3 and JNK phosphorylation are underlined in red and blue, respectively, whereas the corresponding target residues are indicated by arrowheads.

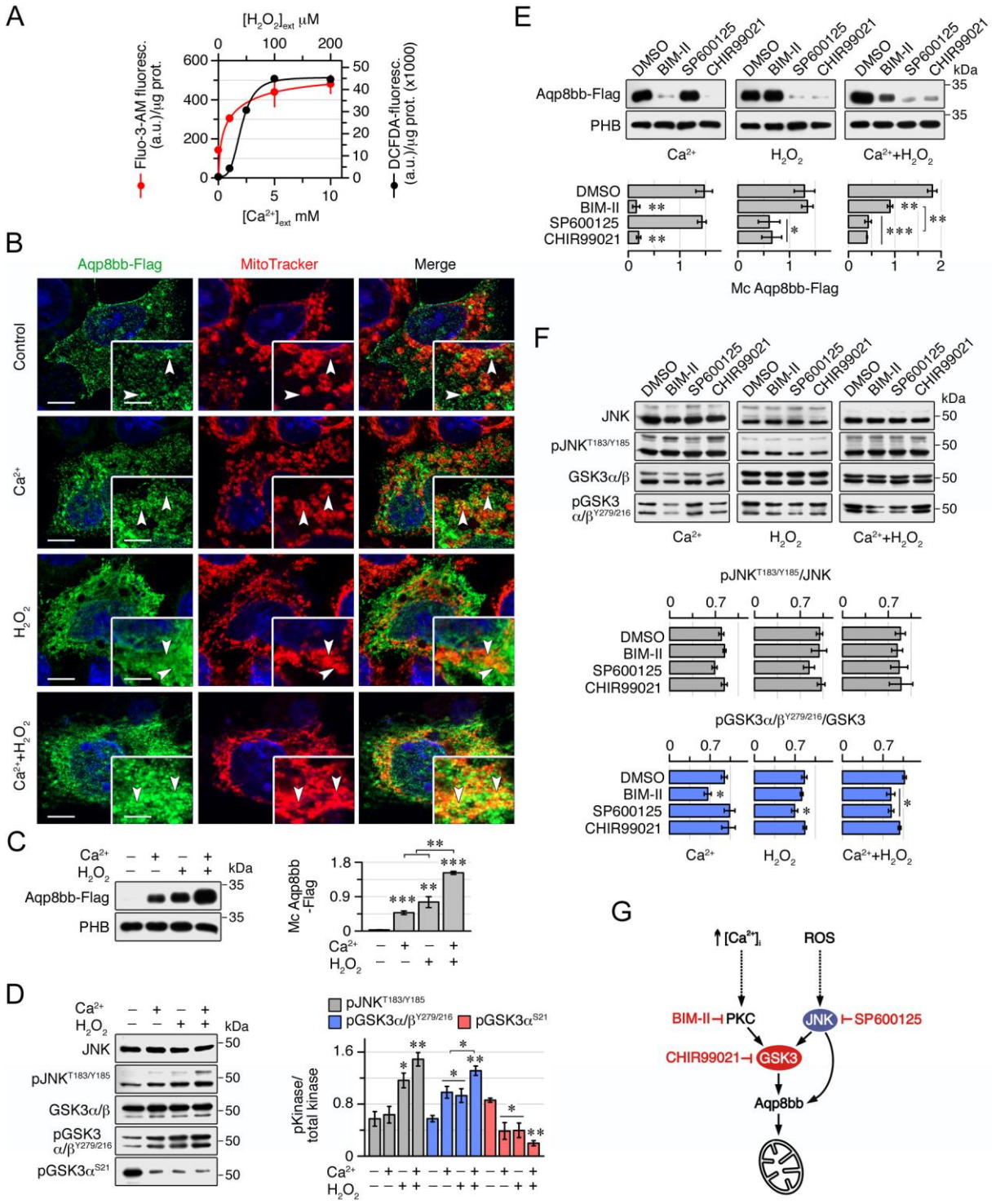

Fig. S8. Ca^{2+}- and ROS-mediated signaling pathways controling Aqp8bb mitochondrial transport in seabream spermatozoa can be replicated in human HepG2 culture cells. (*A*) Dose-response increment (mean ± SEM of 6-8 replicates from one experiment) of $[Ca^{2+}]_i$ (red line) and ROS levels (black line) in HepG2 cells in response to extracellular Ca^{2+} and H_2O_2. (*B*) Double staining of Aqp8bb-Flag and mitochondria in non-treated transfected HepG2 cells or after treatment with Ca^{2+} (10 mM) and/or H_2O_2 (100 µM). Arrowheads indicate co-localized signals. Scale bars, 10 µm (5 µm, insets). (*C*) Immunoblot of mitochondrial Aqp8bb-Flag in cells treated as in *B* (left panel), and corresponding quantitation normalised to PHB (right panel). (*D*) JNK and GSK3 immunoblots (left), and densitometric analysis of phosphorylated forms normalized to the corresponding non-phosphorylated bands (right), in cells treated as in *B*. (*E*) Immunoblot (upper panels) and quantitation (lower panels) of

mitochondrial Aqp8bb in untreated or Ca^{2+} and/or H_2O_2 treated cells in the presence of BIM-II, SP600125 and CHIR99021 inhibitors. (*F*) Immunoblot of kinase activation (upper panels) and corresponding quantitation (lower panels) in cells treated as in *E*. In *C*-*F*, data (mean ± SEM; $n = 3$ separate experiments) are statistically analyzed by one-way ANOVA. ***$P < 0.001$; **$P < 0.01$; *$P < 0.05$, with respect to non-treated cells, or as indicated in brackets. (*G*) Summarized model of the pathways activated in HepG2 cells controlling Aqp8bb mitochondrial transport.

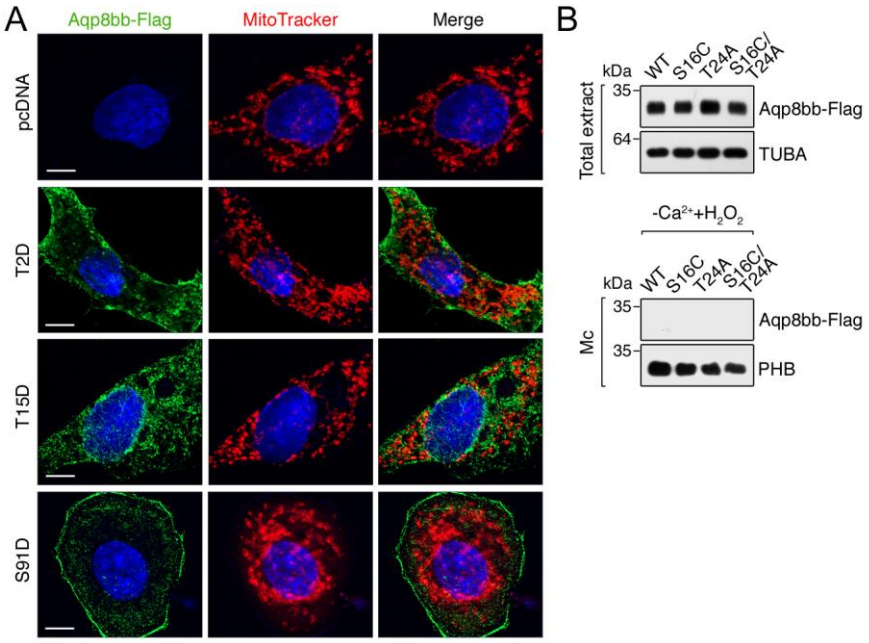

Fig. S9. Effect of seabream Aqp8bb mutants on mitochondrial channel transport in HepG2 cells. (*A*) Double staining of Aqp8bb-Flag (green) and mitochondria (MTR, red) in cells transfected with empty pcDNA vector or transiently expressing Aqp8bb-Flag-T2D, -T15D or -S91D. Scale bars, 10 µm. (*B*) Upper panels, immunoblot of Aqp8bb-Flag-WT and channel mutants preventing Ser^{16} and Thr^{24} phosphorylation, or both, in total protein extracts from HepG2 cells. Tubulin (TUBA) is used as loading control. Lower panels, immunoblot of the same constructs in mitochondrial extracts (Mc), using PHB as control, from cells not to exposed to Ca^{2+} and H_2O_2. Molecular mass markers are on the left.

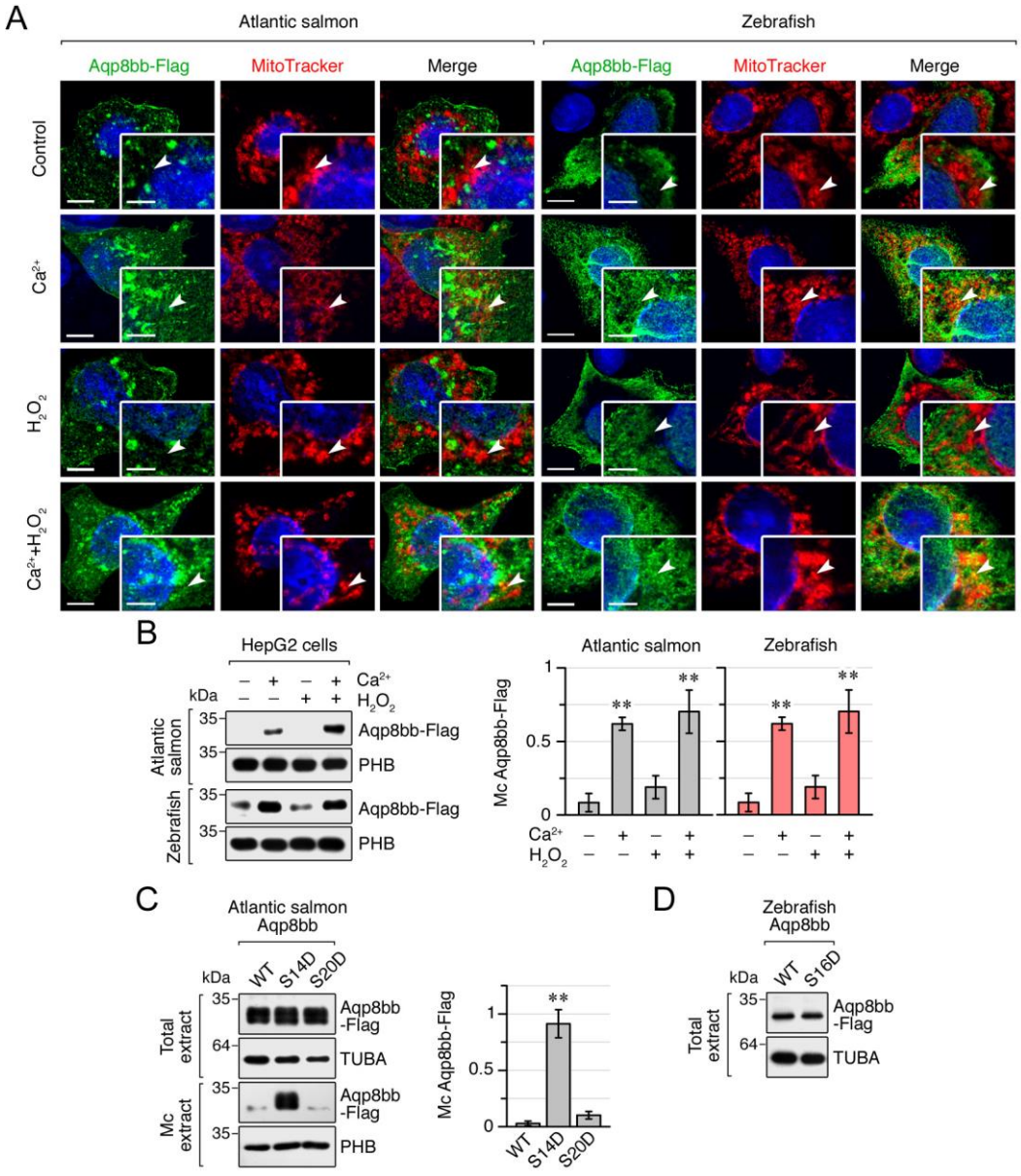

Fig. S10. Transient expression of Atlantic salmon and zebrafish Aqp8bb-Flag in HepG2 cells. (*A*) Double staining of salmon or zebrafish Aqp8bb-Flag (green) and mitochondria (MTR, red) in non-treated HepG2 cells or after external treatment with Ca^{2+} (10 mM) and/or H_2O_2 (100 µM). The arrowheads indicate co-localized signals. Scale bars, 10 µm (insets 5 µm). (*B*) Representative immunoblot of mitochondrial Aqp8bb-Flag (left panels), and corresponding quantitation normalised to PHB (right panels), from HepG2 cells transiently expressing salmon or zebrafish Aqp8bb-Flag-WT and exposed to Ca^{2+} and/or H_2O_2. (*C*) Immunoblot of salmon Aqp8bb-Flag-WT and the Aqp8bb-Flag-S14D and -S20D mutants in HepG2 cells. The left upper panels show the expression of the different channels and tubulin (TUBA), whereas the left lower panels show the accumulation of the constructs in the mitochondria. On the right, is depicted the corresponding mitochondrial quantitation normalised to PHB. Data (mean ± SEN; n = 3 separate experiments) in *B* and *C* are statistically analyzed by one-way ANOVA. $^{**}P < 0.001$, with respect to untreated cells (*B*) or salmon Aqp8bb-Flag-WT (*C*). (*D*) Immunoblot showing the expression levels of total zebrafish Aqp8bb-Flag-WT and the Aqp8bb-Flag-S16D mutant, and of TUBA, in HepG2 cells.

Supplementary Materials and Methods

Animals and sperm collection. Adult gilthead seabream males were raised in captivity at Institut de Recerca i Tecnologia Agroalimentàries (IRTA) aquaculture facilities in San Carlos de la Rápita (Tarragona, Spain) and maintained in the laboratory as previously described (1). Zebrafish and Atlantic salmon were maintained, respectively, at the PRBB Animal Facility (Barcelona, Spain) and the Matredal Aquaculture Research Station (Norway). In seabream and salmon, milt was recovered by abdominal massage from sedated males, whereas sperm were collected from zebrafish by surgical removal of the testis from anesthetized males. Procedures relating to the care and use of animals and sample collection were approved by the Ethics Committee (EC) of IRTA, following the European Union Council Guidelines (86/609/EU), or in accordance with the regulations approved by the governmental Norwegian Animal Research Authority (http://www.fdu.no/fdu/).

Reagents and antibodies. The drugs, enzymes and other compounds used for the different experimens in this study are listed in Table S1, whereas commercial and custom made antibodies employed are described in Table S2. Other reagents were purchased from Merck unless indicated otherwise.

DNA constructs. Full-length cDNAs encoding seabream, Atlantic salmon and zebrafish wild-type Aqp8bb (GenBank accession Nos. DQ889225.1, KC626880.1 and FJ695516.2, respectively), which were Flag-tagged at the N-terminus by PCR, were subloned into the pcDNA3 expression vector. Plasmids encoding dominant-negative forms of human JNK, Jnk1a1(apf) (plasmid # 13846), and *Xenopus laevis* GSK3, pCS2 DN-GSK3-GFP (plasmid # 29681), were purchased from Addgene. Site-directed mutagenesis was carried out using the QuikChange Lightning Site-Directed Mutagenesis Kit (Agilent Technologies). Oligonucleotides were ordered from Thermo Fisher Scientific and constructs were verified by DNA sequencing (Macrogen).

Computational analysis of aquaporin structure. Prediction of kinase-specific phosphorylation residues in seabream, Atlantic salmon and zebrafish Aqp8bb orthologs was carried out using the NetPhos 3.1 Server (http://www.cbs.dtu.dk/services/NetPhos/) (2) and The Eukaryotic Linear Motif resource (http://elm.eu.org/) (3). The three-dimensional structures of the seabream Aqp8bb were built as described previously (4) using the model leverage option in the modeller server (modbase.compbio.ucsf.edu), based upon the *Pichia pastoris* Aqy1 (3GD8) template. The best scoring model was selected using the slow (Seq-Prf, PSI-BLAST) assignment method and rendered with MacPymol (pymol.org).

Sperm treatments and evaluation of motility by CASA. Freshly ejaculated sperm from seabream and salmon was diluted 1:100 in NAM (in mg/ml: 3.5 NaCl, 0.11 KCl, 1.23 $MgCl_2$, 0.39 $CaCl_2$, 1.68 $NaHCO_3$, 0.08 glucose, 1 bovine serum albumine [BSA], pH 7.7; 280 mOsm) (1), or in non-activating diluent 1 (5), using BSA instead of L-α-lecithin (in mg/ml: 8 NaCl, 0.82 KCl, 0.57 Na_2HPO_4, 4 BSA, pH 8; 300 mOsm), respectively. For zebrafish, sperm was isolated by crushing or dissecting the testis in the non-activating SS300 solution (in mg/ml: 8.15 NaCl, 0.67 KCl, 0.11 $CaCl_2$, 0.12 $MgSO_4$, 0.18 glucose, 2.42 Tris-Cl pH 8.0; 300 mOsm) (6) followed by a gentle centrifugation (100 × *g*). Spermatozoa concentration was determined by CASA using the Integrated Semen Analysis System (ISASv1, Proiser) software as previously described (1). In all species, sperm (10^9 cells/ml in the corresponding NAM) was treated with increasing concentrations

of the different kinase inhibitors/activators (0.1, 1, 5 and 10 μM, or with one 10 μM dose), or the vehicle (0.5% DMSO; controls), for 1 h (seabream and salmon) or 15 min (zebrafish) at room temperature, and subsequently activated by 1:10 (seabream and salmon) or 1:3 (zebrafish) dilution in filtered SW (seabream) or deionized water (salmon and zebrafish) for 5 s. The effect of Ca^{2+} or ROS on immotile spermatozoa was tested by exposing NAM-incubated sperm to 10 μM of the different kinase inhibitors for 30 min, and subsequently treated with 3 mM $CaCl_2$ and 10 μM of the Ca^{2+} ionophore A23187 (7), or increasing doses of X-XO (X-XO1: 0.1 mM X + 0.01 U/ml XO; X-XO2: 0.2 mM X + 0.0175 U/ml XO; X-XO3: 0.3 mM X + 0.025 U/ml XO) (8), for another 30 min. In some experiments, seabream sperm was activated in SW in the presence of increasing doses of BAPTA (5, 50 and 500 μM) and/or DPI (1, 5 and 50 μM). For seabream and zebrafish, the percentage of total motile and progressive spermatozoa and VCL, in the presence or absence of kinase inhibitors, were recorded by CASA every 10 s up to 3 min at room temperature (Table S3).

Cell culture. Human embryonic kidney cells 293T (HEK293T, ATCC # CRL-11268) and Hepatocellular carcinoma HepG2 cells (ATCC # CRL-10741) were grown at 37°C in an atmosphere of air/CO_2 [95:5 (v/v)] in Dulbecco's modified Eagle's medium (DMEM) supplemented with 10% v/v fetal bovine serum (FBS), 260 U/ml of penicillin and streptomycin, and 2 mM L-glutamine. At 75% of confluence, cells were transiently transfected in 6-well plates with 5 μg of WT Aqp8bb-Flag and/or 5 μg of the desired constructs, or with 5 μg of the pcDNA3 vector alone, using Lipofectamine 3000 (Invitrogen). The following day, the cells were trypsinized and used for the different experiments. To test the effect of Ca^{2+} and/or H_2O_2 on Aqp8bb trafficking, HepG2 cells were preincubated or not with kinase inhibitors for 1 h at 37ºC and subsequently exposed to increasing doses of $CaCl_2$ (1, 5 or 10 mM) or H_2O_2 (20, 50, 100 or 200 μM) for 30 min.

Reverse transcriptase-PCR (RT-PCR). Total RNA was extracted from different adult tissues, including testis and sperm, using the RNeasy Minikit (Qiagen) including DNAseI treatment, following the manufacturer's instructions. Total RNA (5 μg) was reverse transcribed using 0.5 μg oligo$(dT)_{17}$ primer, 1 mM deoxynucleotide triphosphates (dNTPs), 40 IU RNAse out (Life Technologies Corp.), and 10 IU SuperScript II Reverse Transcriptase enzyme (Life Technologies Corp.) for 1.5 h at 42ºC. The PCR was carried out with 1 μl of the RT reaction in a final volume of 50 μl containing PCR buffer, 0.2 mM dNTPs, 1 IU of Taq polymerase (Roche), and 1 μM of forward and reverse primers (Table S4 and Fig. S2*A*). Reactions were amplified using one 5-min cycle of 95°C; 35 cycles of 95°C for 30 sec, 60°C for 30 sec, and 72°C for 1 min; and a final 7-min elongation at 72°C. PCR products were run on 1% agarose gels and photographed.

Functional expression in *Xenopus laevis* oocytes. Full-length zebrafish Aqp8bb-M1 and -M22 cDNAs were subcloned into the pT7Ts vector for expression in *X. laevis* oocytes (9). The cRNAs for microinjection of oocytes were synthesized with T7 RNA polymerase plus (Ambion) from *Xba*I-linearized plasmids. Isolation of stage V oocytes and microinjection was performed as previously described (9). Oocytes were transferred to modified Bart's solution (MBS; 88 mM NaCl, 1 mM KCl, 2.4 mM $NaHCO_3$, 0.82 mM $MgSO_4$, 0.33 mM $Ca(NO_3)_2$, 0.41 mM $CaCl_2$, 10 mM HEPES, and 25 μg/ml gentamycin, pH 7.5) and injected with 50 nl of distilled water (negative control) or 50 nl of water solution containing 5ng of Aqp8bb-M1 or -M22 cRNA. One day after injection, oocytes were manually defolliculated and subsequently maintained in MBS at 18ºC. The osmotic water permeability (P_f) was determined the following day by transferring the oocytes into 10-fold diluted MBS (20 mOsmol) and oocyte swelling was recorded by video microscopy using

serial images at 2 sec intervals during the first 20 sec using a Nikon Color view video camera coupled to a stereomicroscope (SMZ1000, Nikon Corp., Tokyo, Japan). The P_f values were calculated taking into account the time-course changes in relative oocyte volume ($d(V/V_0)/ dt$), the molar volume of water (V_W = 18 cm^3/ml) and the oocyte surface area (S) using the formula $V_0(d(V/V0)/dt)/(SV_W(Osm_{in} - Osm_{out}))$.

Determination of $[Ca^{2+}]_i$ and ROS Levels. Intracellular Ca^{2+} content in sperm was estimated using the Fluo-3-AM vital dye. Motile and immotile sperm (10^9 cells/ml), previously incubated in the presence or absence of selected drugs for 1 h, were loaded during the last 15 min with a 1:200 diluted solution containing equivalent volumes (1:1) of 1 mM Fluo3-AM in DMSO and 8% NP-40 in 20% DMSO (5 µM Fluo3-AM and 0.3% DMSO final). In some experiments, 10 µM of the Ca^{2+} ionophore A23187 was added at the end of the incubation period for 1 min as above. Sperm were then centrifuged at 1000 × *g* for 1 min and resuspended in fresh NAM. A 15-µl aliquot of the sperm suspension was loaded in each well (10^7 cells/well) of a black 96-well microplate (Nunc F96 MicroWell Black and White Polystyrene Plate; Thermo Fisher Scientific Inc.) and diluted with 135 µl of either NAM or SW for 5 min prior to measurement of the fluorescence intensity at excitation and emission wavelengths of 506 and 526 nm, respectively, using an Infinite M200 microplate reader (Tecan Group Ltd.). The background signal of sperm in NAM or SW not loaded with Fluo3-AM was subtracted from each value.

For ROS determination, sperm cells were loaded with 200 mM of the CM-H_2DCFDA dye for 1 h, during which drugs were added as described above. Sperm was centrifuged 1 min at 1000 × *g*, and resuspended in fresh NAM to wash out the dye. Aliquots of 10 µl were loaded in 96-well plates and diluted 1:10 in NAM or SW prior to measurement of fluorescence intensity as above. The background signal of non-loaded sperm sperm was also subtracted to each value. The same protocols were used to measure Ca^{2+} and ROS in HepG2 cells plated in 96-well plates. In all cases, measurements were carried out in triplicate or quadruplicate.

Isolation of mitochondria from sperm and cultured cells. For mitochondria isolation from spermatozoa, sperm (10^{10} cells/ml) was treated with 250 ng/ml MitoTracker Red and kinase modulators for 1 h, and centrifuged at 700 × *g* during 5 min at room temperature. The pellet was then resuspended in 400 µl of either NAM or SW and the heads and flagellum of spermatozoa were immediately separated by passing the sperm extract 10 times through a capillary (0.5 mm diameter) attached to a 2-ml syringe. The suspension was then placed on top of a sucrose gradient prepared in 2-ml microtubes (400 µl of 2 M sucrose, then 400 µl of 1.5 M sucrose, 400 µl of 1 M sucrose, and finally 400 µl of 0.5 M sucrose), and centrifuged at 14000 × *g* for 60 min at 4ºC. Heads containing mitochondria stained in red were recovered with a micropipette at the 2 M-1.5 M interface (approximately 250 µl) and diluted in 1.25 ml of 0.9% NaCl before centrifuging at 10000 × *g* for 15 min at 4 °C. The pellet was resuspended by pipetting up and down 5 times in 200 µl of the mitochondria homogenization buffer (MHB: 10 mM Tris-HCl pH 7.5, 10 mM KCl, 0.15 mM $MgCl_2$, 1 mM DTT, 1 mM NaF, 1 mM Na_3V0_4, and protease inhibitors [EDTA-free Protease Inhibitor Cocktail Tablets]) and kept on ice for 10 min. Subsequently, 30 µl of 2 M sucrose was added to the extract (to obtain a final concentration of 0.25 mM sucrose) and the suspension was gently vortexed and centrifuged at 1200 × *g* for 5 min at 4°C. The supernatant was transferred to a new 1.5-ml microtube and centrifuged again at 1200 × *g* for 5 min at 4ºC. Finally, the supernatant was transferred to a new 1.5-ml tube and centrifuged at 7000 × *g* for 10 min at 4ºC. The resulting pellet was resuspended in 100 µl of the mitochondria resuspension buffer (MRB: 10 mM Tris-HCl pH 6.7, 0.15 mM $MgCl_2$, 0.25 mM sucrose, 1 mM DTT, 1 mM NaF, 1 mM Na_3V0_4, plus protease inhibitors) and

centrifuged at 9500 × *g* for 5 min at 4ºC. The final mitochondrial pellet was used for H_2O_2 uptake assays (see below), the isolation of inner mitochondrial membranes as previously described (10), or immunoblotting. For the later, the pellet was resuspended in 50 µl of PBS plus protease inhibitors, phosphatase inhibitor cocktail 2, 1 mM NaF, and 1 mM Na_3V0_4. The protein content was measured with a NanoDrop 2000c spectrophotometer and the volume adjusted to obtain a concentration of 2.5 µg protein/µl. Then, the sample was mixed with 2 × Laemmli sample buffer plus 0.1 M DTT, and boiled at 95ºC for 10 min before freezing in liquid nitrogen and storage at -80ºC until Western blot analysis.

Mitochondria from HepG2 cells were isolated after 1 h incubation at 37ºC with MitoTracker Red, with or without kinase inhibitors and in the presence/absence of $CaCl_2$ and/or H_2O_2. DMEM media was replaced in each of the 6-well plate with 1 ml of lysis buffer (10 mM NaCl, 1.5 mM $MgCl_2$, 10 mM Tris HCl, pH 7.5, 1 mM DTT) and cells were mixed using a shaker during 5 min in order to break their membranes and detach them from the plate. Cells were then scrapped and the resulting suspension was homogenized with a syringe before adding 1 ml of 2 × homogenization buffer (210 mM mannitol, 70 mM sucrose, 5 mM Tris-HCl, pH 7.5, 10 mM HEPES pH 7.5, and 1 mM EDTA). The extract was transferred to a 2-ml microtube and cellular debris were pelleted by three times centrifugation at 1200 × *g* for 5 min at 4ºC. The supernatant containing the mitochondrial extract was centrifuged at 10000 × *g* for 10 min at 4ºC. The mitochondrial pellet was resuspended in 1 × Laemmli sample buffer containing 0.1 M DTT, and immediately heated at 95°C for 10 min.

Mitochondrial H_2O_2 uptake. The mitochondria extracted from spermatozoa as described above were tested for H_2O_2 uptake using 300 µM of external H_2O_2 as previously described (10). Measurements were carried out in triplicate.

Protein extraction from sperm and cultured cells. Sperm (10^9 cell/ml) were centrifugated for 1 min at 1000 × *g* and the pellet immediately resuspended in a kinase extraction buffer (50 mM Tris/HCl pH 7.5, 150 mM NaCl, 1% Triton X100, 1% sodium deoxycholate, 1 mM EGTA, 0.4 mM EDTA, 1 mM Na_3VO_4, 1 mM NaF, and protease inhibitors), vortexed for 1 min, and kept on ice for 5 min. After sonication at 15% amplitude for 5 s and centrifugation at 14000 × *g* for 10 min at 4ºC, the supernatant was removed and its protein concentration was measured by Bradford and adjusted to 6 µg protein/µl. The supernatant was then mixed with 4 × Laemmli sample buffer with DTT supplemented with protease inhibitors, 2 mM Na_3VO_4, and 2 mM NaF, and 4 × phosphatase inhibitor cocktail 2, to obtain a final concentration of 4 µg protein/µl. Samples were heated at 95ºC for 10 min, frozen in liquid nitrogen and stored at -80ºC until immunoblotting.

For protein extraction from HepG2 cells, transfected cells grown in six-well plates were tripsinized and transferred to a 1.5-ml microtube and centrifuged at 500 × g for 5 min. The pellet was resuspended in 1 ml of radioimmunoprecipitation assay (RIPA) buffer (150 mM NaCl, 50 mM Tris pH 8.0, 1.0% Triton X-100, 0.5% sodium deoxycholate, 0.1% SDS, supplemented with 1 mM NaF, 1 mM Na_3VO_4, protease inhibitors, and 80 U benzonase), vortexed, and incubated for 5 min on ice. The samples were centrifuged at 14000 × *g* at 4ºC for 2 min, and the supernatant was mixed with 2 × Laemmli sample buffer with DTT and heated at 95ºC for 10 min. Samples were frozen and stored as indicated above.

Protein extraction of total membranes from *X. laevis* oocytes. Oocytes were homogenized in HbA buffer (20 mM Tris, pH 7.4, 5 mM $MgCl_2$, 5 mM NaH_2PO_4, 1 mM EDTA, 80 mM sucrose, and cocktail of protease inhibitors [Mini EDTA-free; Roche]) and total membranes were isolated as previously described (11).

Immunoprecipitation. HEK293T and HepG2 transfected cells were lysed in an immunoprecipitation buffer (50 mM Tris-Hcl pH 7.4, 150 mM NaCl, 1 mM EDTA, 1 mM EGTA, 5 mM $MgCl_2$, 1 mM NaF, 1 mM Na_3VO_4, 0.5% Triton X-100, and protease inhibitors). An aliquot (10%) of the extract was collected as "input" and mixed with 2 × Laemmli + DTT supplemented with protease inhibitors, 2 mM Na_3VO_4, and 2 mM NaF. The remaining extract was mixed with activated G-protein beads (Pure Proteome™ Protein G Magnetic Beads) coupled to seabream Aqp8bb antibody or rabbit anti-Flag antibody, or rabbit IgG as negative control, following manufacturer's instructions, and incubated overnight at 4°C under constant agitation. The beads were further washed three times with PBST, eluted in 50 µl of RIPA buffer, and mixed with 4 × Laemmli supplemented with protease and phosphatase inhibitors.

In Vitro Phosphorylaton Assays. Immunoprecipitation eluates from cultured cells were dissolved on ice with a kinase assay buffer (25 mM MOPS, pH 7.2, 12.5 mM β-glycerophosphate, 25 mM $MgCl_2$, 5 mM EGTA, 2 mM EDTA. 0.1 mM Na_3VO_4 and 0.25 mM DTT), and diluted 5-fold with a solution containing 50 ng/ml BSA, 200 µM ATP, and 50-400 ng (0.04-0.33 µM) of rGSK3β or 200 ng of rJNK1 (0.11 µM) or rPKCα (0.08 µM) (Table S1). The mixture was incubated 30 min at 30°C and the reaction terminated by adding Laemmli sample buffer and heating at 95°C for 10 min. Samples were subsequently processed for immunoblotting.

Immunoblotting. Laemmli-mixed protein samples were heated at 95ºC for 10 min and subjected to 12% sodium dodecyl sulfate polyacrylamide gel electrophoresis (SDS-PAGE), and blotted onto Immun-Blot nitrocellulose 0.2 µm Membrane (Bio-Rad Laboratories), as previously described (1). Membranes were blocked with 5% nonfat dry milk or 3% BSA in TBST (20 mM Tris, 140 mM NaCl, 0.1% Tween, pH 8) for 1 h at room temperature, and subsequently incubated overnight at 4ºC with the selected antibody diluted in TBST with 5% milk or 3% BSA as listed in Table S2. Bound antibodies were detected with horseradish peroxidase-coupled anti-mouse, rabbit or goat secondary antibodies (Table S2) diluted as above, and reactive protein bands were revealed using Immobilon™ Western chemiluminescent HRP substrate. For the semi-quantitative determination of Aqp8bb or kinase abundance in the mitochondria or total extracts, respectively, under the different treatments, the intensity of the immunoreactive bands was scored by densitometry using the Quantity-One software (Bio-Rad Laboratories Inc.), and normalized to that of the reference proteins prohibitin or alpha-tubulin. Quantitation of Ser and Thr phosphorylation of Aqp8bb-Flag was normalised to the total immunoprecipitated protein.

Immunofluorescence microscopy of sperm and cultured cells. Spermatozoa labelled with MitoTracker and treated as described above were attached to UltraStick/UltraFrost Adhesion slides (Electron Microscopy Sciences) at room temperature as previously described (1), fixed in 4% paraformaldehyde (PFA) for 5 min, and subsequently permeabilized using PBST (137 mM NaCl, 2.7 mM KCl, 100 mM Na_2HPO_4, 2 mM KH_2PO_4, pH 7.4, 0.1% Triton X-100) for 10 min. Slides were blocked in 5% normal goat serum plus 0.1% BSA in PBST for 1 h, and incubated with the antibodies at different dilutions (Table S2) overnight at 4°C in PBST. After washing, sections were incubated with the corresponding Alexa Fluor 488-conjugated secondary antibodies (Table S2) for 1 h at room temperature, washed in PBS, and counterstained with 4',6-diamidino-2-phenylindole (DAPI; 1:5000) for 3 min in PBS to stain the nuclei. The sections were mounted with fluoromount aqueous anti-fading medium, and examined and photographed with a Zeiss Axio Imager Z1/ApoTome fluorescence microscope (Carl Zeiss Corp.). Images from negative control sections were taken with the same fluorescence intensity and exposure

times than those used for the positives. To determine the percentage of spermatozoa showing Aqp8bb mitochondrial localization, the number of spermatozoa displaying co-localization of Aqp8bb and MitoTracker signals was scored in at least 100 spermatozoa per ejaculate or pool.

For immunofluorescence microscopy on cultured cells, cells attached to round coverslips were fixed in methanol during 6 min at -20ºC, and subsequently in acetone for 30 s. Cells were washed twice in PBS and then permeabilized with PBST for 10 min. The blocking step and incubation with primary and secondary antibodies was carried out as described above, except that the counterstaining with DAPI was used at 1:3000 dilution for 10 min.

Immunofluorescence microscopy on testis sections. Zebrafish and Atlantic salmon testis explants, previously incubated for 1 h with 250 ng/ml MitoTracker® Red CMXRos (Invitrogen), were fixed in 4% paraformaldehyde (PFA) for 6 h, washed, dehydrated, and embedded in Paraplast Plus®. Sections (7 µm) were blocked in 5% goat serum and 0.1% BSA in PBS with 0.1% Tween-20 (PBST) for 1 h, and incubated with PBS containing 0.2%Triton X-100 for 10 min at room temperature. Incubation with the primary antibodies diluted in PBS (Table S2) was performed overnight at 4°C. Slides carrying adjacent sections of the testis were incubated with the antibodies previously adsorbed with the respective immunizing peptides as negative controls. After washing, sections were probed with an Alexa 488-coupled anti-rabbit IgG secondary antibody (Table S2) for 1 h at room temperature. The nuclei were counterstained with 4',6-diamidine-2'-phenylindole dihydrochloride (DAPI) and mounted with fluoromount aqueous anti-fading medium. Sections were examined and photographed with a Zeiss Axio Imager Z1/ApoTome fluorescence microscope (Carl Zeiss Corp.).

Statistics. Results are expressed as the means ± SEM. For seabream and salmon sperm, experiments were carried out on three to eight different males (one ejaculate per male), whereas in the case of zebrafish, experimens were done on five to seven males or on three pools each containing sperm from five different males. Sperm kinetics analysis by CASA were run in triplicate for each ejaculate/pool. For cultured cells, data were obtained from three independent experiments. Comparisons between two independent groups were made by the two-tailed unpaired Student's *t*-test. The statistical significance among multiple groups was analyzed by one-way ANOVA, followed by the Tukey's multiple comparison test, or by the non-parametric Kruskal-Wallis test and further Dunn's test for nonparametric post hoc comparisons, as appropriate. Time-course curves of sperm kinetic parameters were compared by the Mann-Whitney *U* test. Percentages were square root transformed previous analyses. Statistical analyses were carried out using the SigmaPlot software v12.0 (Systat Software Inc.) and GraphPad Prism v8.4.3 (686) (GraphPad Software). In all cases, statistical significance was defined as $P < 0.05$ (*), $P < 0.01$ (**), or $P < 0.001$ (***).

Table S1. Drugs, enzymes and other compounds used for the different experimens in this study

Compound	Abbreviation	Vendor	Catalog no.	Activity
Anisomycin	ANS	Merck	A9789	Inducer of JNK and p38 MAPK phosphorylation
1,2-Bis(2-Aminophenoxy)ethane-N,N,N′,N′-tetraacetic acid	BAPTA	Invitrogen	B6769	Cell-permeant chelator, highly selective for Ca^{2+}
Bisindolylmaleimide II	BIM-II	Santa Cruz Biotechnology	sc-221366	ATP-competitive PKC subtypes inhibitor
Calcium Ionophore A23187	A23187	Merck	C7522	Increases the ability of Ca^{2+} to cross biological membranes
Calphostin C	Cal-C	Santa Cruz Biotechnology	sc-3545	Inhibitor of PKC that targets the regulatory domain
CHIR99021	CHIR99021	Merck	SML1046	Inhibitor of GSK3 kinetic activity
CM-H_2DCFDA	DCFDA	Molecular Probes	C6827	Indicator for ROS in cells
Diphenyleneiodonium chloride	DPI	Merck	D2926	Inhibitor of NADPH oxidase
Doramapimod	BIRB796	Selleck Chemicals	S1574	Inhibitor of kinetic activity and phosphorylation of p38 MAPK
Fluo-3, AM	Fluo-3-AM	Invitrogen	F14218	Cell permeable Ca^{2+} indicator
GNF-7	GNF-7	Merck	SML1501	Ras signaling inhibitor; inhibits Ack1 and GCK
H-89 dihydrochloride hydrate	H-89	Merck	B1427	ATP-competitive PKA inhibitor
IgG from rabbit serum	IgG	Merck	I5006	Immunoglobulin G
Mito-TEMPO	-	Santa Cruz Biotechnology	sc-221945	Mitochondria-targeted antioxidant
MitoTracker™ Red CMXRos	MTR	Molecular Probes	M-7512	Mitochondria-specific, red-fluorescent dye
MK-2206 dihydrochloride	MK2206	Selleck Chemicals	S1078	Allosteric inhibitor of AKT, and activator of GSK3
NG25 trihydrochloride	NG25	Merck	SML1332	ATP-competitive TAK1 and GCK inhibitor
NQDI 1	NQDI-1	Tocris Bioscience	4429	ASK1 inhibitor
PD 98,059	PD98059	Merck	P215	Inhibitor of MEK/MKK phosphorylation
Phorbol 12-myristate 13-acetate	PMA	Merck	P8139	Analog of diacylglycerol, the physiological activator of PKC
4α-Phorbol 12-myristate 13-acetate	4α-PMA	Merck	P148	Negative control for PMA activation of PKC
Recombinant JNK1	rJNK1	Merck	J2455	JNK1 active, GST tagged from mouse
Recombinant GSK3β	rGSK3β	Merck	G4296	GSK3β active, His tagged from human
Recombinant PKC-α	rPKCα	Merck	SRP5251	PKC-α active, GST tagged from *Xenopus sp.*
SB 202190	SB202190	Merck	S7067	ATP-competitive p38 MAP kinase inhibitor
SH-5	SH-5	Santa Cruz Biotechnology	sc-205973	Inhibitor of AKT activation
SP 600125	SP600125	Merck	S5567	ATP-competitive JNK inhibitor
Xanthine	X	Merck	X4002	Purine base
Xanthine Oxidase	XO	Merck	X1875	Generates ROS following the oxidation of xanthine

Table S2. Antibodies used in this study

Antibody/UniProt accession no.	Host species	Vendor	Catalog no.	Working dilution[a]		
				IB	IF	IP
Seabream Aqp8bb/C7S301	Rabbit	Custom made (1)	-	1:1000	1:500	1:500
Atlantic salmon Aqp8aa/S5RRC8	Rabbit	Custom made (12)	-	1:1000	-	-
Atlantic salmon Aqp8ab/S5R5I0	Rabbit	Custom made (12)	-	1:1000	-	-
Atlantic salmon Aqp8bb/C0HB60	Rabbit	Custom made (12)	-	1:1000	1:400	-
Zebrafish Aqp8bb/D3U0R1	Rabbit	Custom made, this study[b]	-	1:1000	1:400	-
ASK/Q99683	Rabbit	Signalway Antibody	21134	1:1000	-	-
ASK1(pS^{966})/Q99683	Rabbit	Signalway Antibody	11179	1:1000	-	-
Flag, clone M2	Mouse	Merck	F3165	1:1000	1:1000	1:500
Flag	Rabbit	Merck	F7425	1:1000	1:1000	1:500
GSK3a/b/ P49840,P49841	Mouse	Santa Cruz Biotechnology	sc-7291	1:1000	-	-
GSK3a/b (pY$^{279/216}$)/P49840,P49841	Rabbit	Signalway Antibody	11301	1:1000	-	-
GSK3a (pS^{21})/ P49840	Rabbit	Signalway Antibody	11007	1:500	-	-
GSK3b (pS^{9})/ P49841	Mouse	Santa Cruz Biotechnology	sc-373800	1:500	-	-
JNK (JNK1/3)/ P45983	Goat	Santa Cruz Biotechnology	sc-474	1:1000	-	-
JNK1/2/3(pT^{183}/Y^{185})/ P45983,P45984,P53779	Mouse	Santa Cruz Biotechnology	sc-6254	1:200	-	-
MEK-4/P45985	Rabbit	Signalway Antibody	41138	1:500	-	-
MEK-4 (pT^{261})/ P45985	Rabbit	Signalway Antibody	12208	1:500	-	-
Phosphoserine (5B12)	Mouse	Signalway Antibody	12828	1:500	-	-
Phosphothreonine (H-2)	Mouse	Santa Cruz Biotechnology	sc-5267	1:500	-	-
Prohibitin/Q7T1D8	Rabbit	GeneTex	GTX124491	1:2000	-	-
Rabbit IgG Horseradish Peroxidase	Goat	Bio-Rad	172-1019	1:5000	-	-
Mouse IgG Horseradish Peroxidase	Goat	Bio-Rad	172-1011	1:5000	-	-
Goat IgG Horseradish Peroxidase	Rabbit	Merck	A8919	1:5000		
Rabbit IgG Alexa Fluor 488	Goat	Invitrogen	A-11008	-	1:1000	-
Mouse IgG Alexa Fluor 488	Goat	Invitrogen	A-11001	-	1:1000	-
α-Tubulin, clone DM1A/F1NW97	Mouse	Merck	T9026	1:25000	-	-

[a] IB: immunoblotting; IF: immunofluorescence; IP: immunoprecipitation.

[b] A rabbit polyclonal antisera for zebrafish Aqp8bb is raised against a synthetic peptide, LGDNDTRVVMK, corresponding to the C-terminus amino acid residues of the corresponding predicted protein (Agrisera AB, Vännäs, Sweden). The antiserum is purified by affinity chromatography against the synthetic peptide, and its specificity is confirmed by ELISA, and by heterologous expression of the Aqp8bb protein in *Xenopus laevis* oocytes.

Table S3. Settings of the CASA system

Parameters for sperm tracking	Settings
Counting chamber	ISAS R2C10
Camera	ISAS 782C
Frames	25 frames per s
Image resolution	768 x 576 pixels
Magnification	× 20 phase
Particle area	0-30 µm
Connectivity[a]	14 µm
Cuvilinear velocity (VCL)	>10 µm/s
Path straightness (STR)	>10%
Linearity (LIN)	>10%
Wobble (WOB)	>10%
Max. velocity (for tracking)	500 µm/s
Average path velocity (VAP)	>10 µm/s

[a] Connection of the sperm head tracks within different frames.

Table S4. RT-PCR primers for Atlantic salmon *aqp8aa*, *-8ab* and *-8bb* paralogs

Transcript	GenBank accession no.	Direction	Primer (5' to 3')
aqp8aa	KC626878	Forward	CAAAGACGGAGCTCTTCACC
		Reverse	CTGACGCACACACTCACAGA
aqp8ab	KC626879	Forward	CGGCGTTTACTATCCTCCAA
		Reverse	TCCACAGTGACTTGCATAGGA
aqp8bb	KC626880	Forward	CCCTGCTGCAATCACAAGAT
		Reverse	CAACAGCGGTAATCTCAGACC

SI References

1. F. Chauvigné, M. Boj, S. Vilella, R. N. Finn, J. Cerdà, Subcellular localization of selectively permeable aquaporins in the male germ line of a marine teleost reveals spatial redistribution in activated spermatozoa. *Biol. Reprod.* **89**, 37 (2013).
2. N. Blom, T. Sicheritz-Ponten, R. Gupta, S. Gammeltoft, S. Brunak, Prediction of post-translational glycosylation and phosphorylation of proteins from the amino acid sequence. *Proteomics* **4**, 1633-1649 (2004).
3. M. Gouw, S. Michael, H. Sámano-Sánchez, M. Kumar, A. Zeke *et al.*, The eukaryotic linear motif resource - 2018 update. *Nucleic Acids Res.* **46**, D428-D434 (2018).
4. F. Chauvigné, O. Yilmaz, A. Ferré, P. G. Fjelldal, R. N. Finn *et al.*, The vertebrate Aqp14 water channel is a neuropeptide-regulated polytransporter. *Commun. Biol.* **2**, 462 (2019).
5. R. K. Gallant, G. F. Richardson, M. A. McNiven, Comparison of different extenders for the cryopreservation of Atlantic salmon spermatozoa. *Theriogenology* **40**, 479-486 (1993).
6. J. L. Matthews, J. M. Murphy, C. Carmichael, H. Yang, T. Tiersch *et al.*, Changes to extender, cryoprotective medium, and *in vitro* fertilization improve zebrafish sperm cryopreservation. *Zebrafish* **15**, 279-290 (2018).
7. M. Boj, F. Chauvigné, J. Cerdà, Coordinated action of aquaporins regulates sperm motility in a marine teleost. *Biol. Reprod.* **93**, 40 (2015).
8. M. Hagedorn, M. McCarthy, V. L. Carter, S. A. Meyers, Oxidative stress in zebrafish (*Danio rerio*) sperm. *PLoS One* **7**, e39397 (2012).
9. Deen, P. M. T. et al. Requirement of human renal water channel aquaporin-2 for vasopressin-dependent concentration of urine. *Science* **264**, 92-95 (1994).
10. F. Chauvigné, M. Boj, R. N. Finn, J. Cerdà, Mitochondrial aquaporin-8-mediated hydrogen peroxide transport is essential for teleost spermatozoon motility. *Sci. Rep.* **5**, 7789 (2015).
11. Kamsteeg, E. J. & Deen, P. M. Detection of aquaporin-2 in the plasmamembranes of oocytes: a novel isolation method with improved yield and purity. *Biochem. Biophys. Res. Commun.* **282**, 683-690 (2001).
12. Engelund, M.B., Chauvigné, F., Christensen, B.M., Finn, R.N. Cerdà, J. & Madsen, S.S. Differential expression and novel permeability properties of three aquaporin 8 paralogs from seawater-challenged Atlantic salmon smolts. *J. Exp. Biol.* **216**, 3873-3885 (2013).